



**Politecnico
di Torino**

Politecnico di Torino

Ingegneria energetica e nucleare – Renewable energy systems

A.a. 2022/2023

Sessione di Laurea marzo/aprile 2023

Experimental analysis of polymeric membranes for CO₂/CH₄ separation in biogas upgrade

Relatori:

Prof. Santarelli Massimo
PhD. Cannone Salvatore F.

Candidato:

Gabriele Marrocchino

Ringraziamenti

Vorrei dedicare questa sezione dell'elaborato alle persone che mi sono state vicine in questo percorso di crescita.

Voglio innanzitutto ringraziare il professor Massimo Santarelli, relatore di questa tesi. Grazie a lui ho avuto la possibilità di conoscere il mondo della ricerca e comprendere maggiormente le attività ad essa legate.

Ringrazio il Dottore di Ricerca Salvatore Cannone, correlatore di questo elaborato, per la sua pazienza, per i suoi indispensabili consigli e per le conoscenze trasmesse durante tutto il percorso di stesura.

Vorrei ringraziare Giovanni, Giulia e Matteo, compagni di laboratorio e persone fantastiche, con i quali ho condiviso una parte importante del mio corso di studi. Grazie ai miei compagni di corso Pietro, Filippo e Lilia per avermi fatto amare il lavoro di squadra ed avermi accompagnato nel percorso di laurea.

Un ringraziamento speciale va alle Compenetrazioni. Sono immensamente felice di raggiungere un ulteriore traguardo con voi al mio fianco, grazie per avermi accompagnato in questi anni. Ringrazio Andrea, le nostre sessioni musicali hanno contribuito ad accrescermi, in particolar modo sul profilo creativo. Ringrazio Enrico, mi hai sempre incoraggiato e confortato nel momento del bisogno. Ringrazio Andrea e Noemi, persone stupende che con il loro calore mi hanno sempre fatto sentire a casa.

Sarò eternamente grato alla mia famiglia. Grazie a Diana e Francesco, genitori stupendi, mi sento fortunato ad esser cresciuto con voi. Grazie a Rosa e Alberto per avermi ascoltato nel momento del bisogno ed aver condiviso gioie e dolori. Un immenso grazie ai nonni Salvatore e Vita, sarete sempre nel mio cuore.

Infine vorrei ringraziare Elena. Grazie per tutto il tempo che mi hai dedicato. Grazie per avermi aiutato nelle scelte più difficili. Grazie per esserci sempre stata.

Index

1 – General introduction.....	1
1.1 – EU energy security during Russia invasion	3
1.2 – Circular economy applied in CO ₂ field.....	4
1.3 – Thesis objectives	6
2 – Biomethane as substitute of fossil methane	8
2.1 – NG trends in different scenarios.....	8
2.2 – Biogas and biomethane in EU	9
3 – Biomethane upgrade systems	13
3.1 – Biogas composition, production and cleaning processes	13
3.2 – Absorption.....	16
3.2.1 – High pressure water scrubbing (HPWS)	17
3.2.2 – Organic physical scrubbing.....	18
3.2.3 – Amine scrubbing	18
3.2.4 – Inorganic solvent scrubbing	19
3.3 – Adsorption.....	19
3.3.1 – Pressure swing adsorption.....	19
3.3.2 – Temperature swing adsorption	20
3.3.3 – Electrical swing adsorption	21
3.4 – Cryogenic separation.....	21

4 – Membranes for CO ₂ separation	23
4.1 – Materials for membrane technologies	23
4.1.1 – Polymeric membranes	23
4.1.2 – Inorganic membranes	27
4.1.3 – Mixed matrix membranes (MMM)	28
4.2 – Transport mechanisms.....	29
4.2.1 – Transport in non porous (dense) membranes	29
4.2.2 – Transport in porous membrane	32
4.3 – Technical limitations	33
4.3.1 – Robeson upper bound related to dense polymeric membranes	33
4.3.2 – Swelling.....	34
4.3.3 – Plasticization	35
5 – Experimental setup	37
5.1 - Tested membrane	37
5.1.1 – Matrimid.....	37
5.1.2 - PES-WC.....	38
5.1.3 - PEEK-WC.....	39
5.2 – Experimental CO ₂ capture system test rig.....	40
5.2.1 - Closed volume test.....	42
5.2.2 - Open system test	43
6 - Data filtering and evaluation.....	45
6.1 - Raw data analysis in closed volume case	45
6.1.1 - Acquisition transcription.....	45

6.1.2 – Noise and precision evaluation	46
6.2 - Data filtering	48
6.3 - Permeability calculation in closed volume	50
6.4 – Permeability calculation in open volume	50
7 – Results	52
7.1 – Matrimid.....	52
7.2 - PES-WC	53
7.2.1 – PES-WC without cyclodextrin nanosponge.....	53
7.2.1 – PES-WC with cyclodextrin nanosponge	54
7.3 - PEEK-WC.....	56
7.4 – Comparison between tested membranes	58
8 – Conclusions	59
9 – Bibliography.....	61

1 – General introduction

Many datasets recorded in the last century an increase in global average surface temperature (such as hadCRUT4.6, NOAA GlobalTemp, GISTEMP and Cowtan-Way) with respect to the pre-industrial period: temperature increase between 1850-1900 to 2006-2015 was observed to be between 0.79°C and 0.98°C with an average of 0.87°C [1]. This change is mainly linked to human activities, i.e. hydrocarbon oxidation, cement production, biomass burning and deforestation, which have in common emission of CO₂ as a product. Looking at the world CO₂ concentration in the past years an important anomaly in nowadays period can be observed.

CARBON DIOXIDE OVER 800,000 YEARS

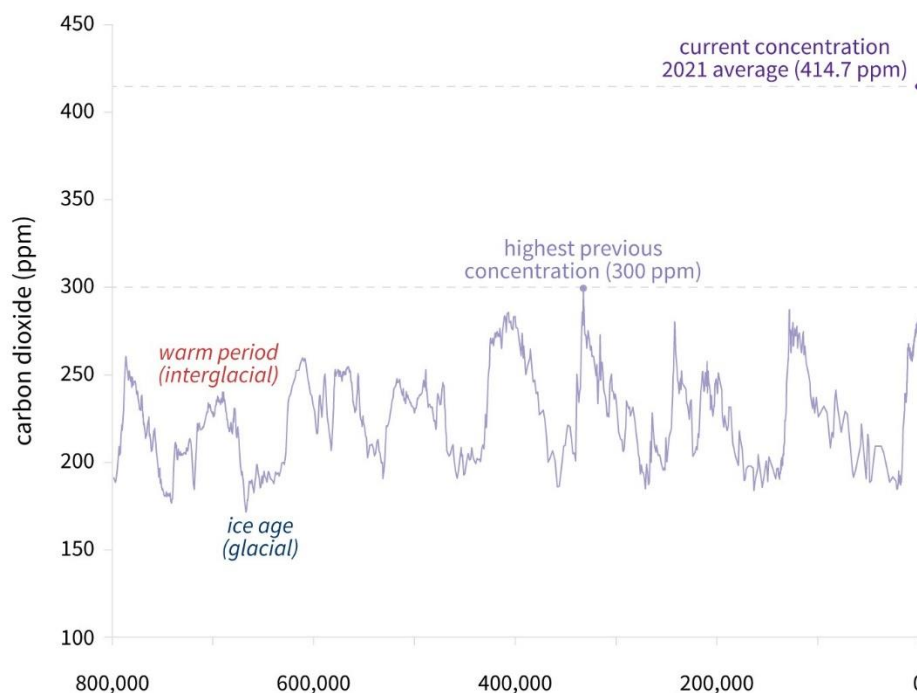


Figure 1: change in atmospheric carbon dioxide through the years. Ages are mainly divided by interglacial and glacial ages, characterized by warm and cold period respectively with higher or lower concentration of carbon dioxide [2].

Atmospheric carbon dioxide before human activities had a peak in concentration with a value of 300 ppm: it had an irregular trend, but most of the time laid between 200 ppm and 250 ppm. In 1850 (pre-industrial period) CO₂ concentration was 280 ppm and both carbon dioxide value and mean global temperature in that year were set as the reference values for many studies. After many publications about the relationship between carbon dioxide and mean global temperature, different policy makers shared the necessity to establish common goals to deal with climate change. Nowadays the most important collaboration about this global issue is the Paris Agreement. The Paris Agreement is a legally binding international treaty on climate change. It was adopted by 196 Parties at COP 21 in Paris, on 12 December 2015 and entered into force on 4 November 2016 [3]. Its goal is to limit temperature increase well below 2°C,

aiming not to overcome 1.5°C compared to the pre-industrial period, by limiting the carbon dioxide emission: this 0.5°C difference would bring less drastic change in the ecosystem with respect to the 2°C scenario. IPCC (International Panel on Climate Change) studied the main differences between these two scenarios, stating that, with less than 1°C difference, global climate change has already had an impact on organisms and ecosystems, as well as on human systems and well-being [1]. Also, it has to be taken into account that any increase in temperature is a mean between different locations, hence with the same scenario some places could see an higher or lower change in temperature with respect to the mean one and have higher or lower impact on ecosystem and organisms: regarding hot extremes, for the warm season the most subjected areas would be the mid-latitudes ones with an increase up to 3°C in 1.5°C scenario, while for cold season the high latitudes regions would see an increase of temperature up to 4.5°C. Moreover, a 1.5°C scenario is a long-time temperature goal which should include a reduction of carbon dioxide in atmosphere after a net zero emission.

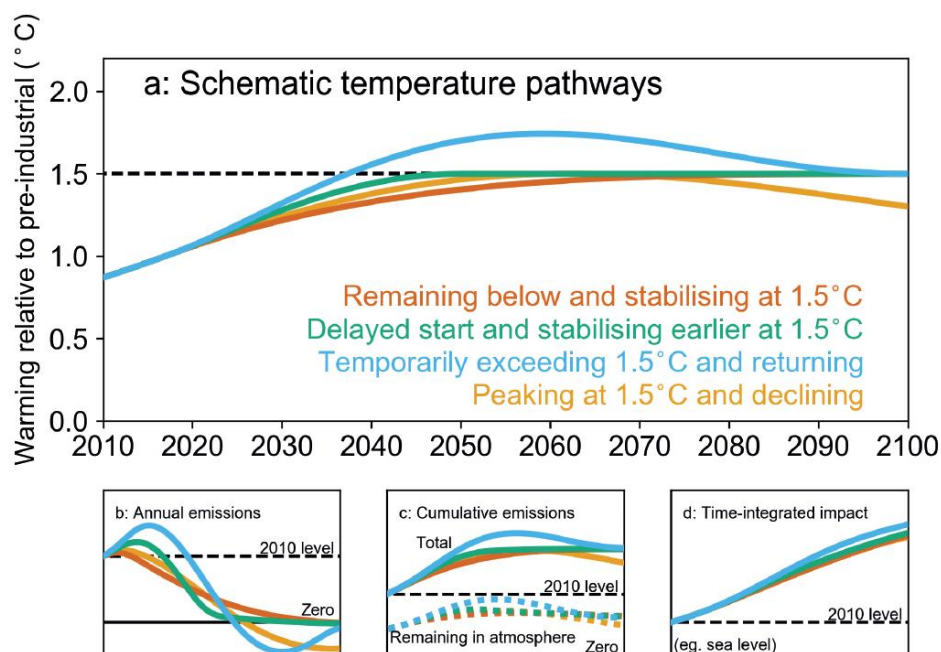


Figure 2: comparing different scenarios with respect to time. Each graph is composed by four lines which represent the different possible pathways in order to be under 1.5°C at the end of the century. In graph a) it is represented the mean global temperature, in graph b) the associated annual emissions, with comparison to the 2010 level and the net-zero one, in graph c) it is represented the integration over time of the graph b), while in graph d) there is a time-integrated impact, in this case the sea level has been taken as a reference [1].

Overshooting the 1.5°C would put in risk natural and human systems, with long-lasting and irreversible risks: the damage would be proportional both to the magnitude of the overshoot and time passed above the 1.5°C limit. Most important risks are extreme drought, precipitation deficits, water availability, heat waves and flood hazard. The ocean has already absorbed almost a third of the carbon dioxide emitted by humans, which results in water acidification and reduction of ecosystem, and with the increase in the next years of atmospheric carbon dioxide concentration this could only get worse; reductions in yields of maize, rice, wheat and other

cereal crops is expected particularly in the sub-Saharan, Southeast Asia and Central and South America regions.

1.1 – EU energy security during Russia invasion

Two of the most common point when making policies about greenhouse gases are utilization of renewable energy systems and energy efficiency [4], but in order to achieve these objectives, a transition between fossil fuels and clean energy sources is needed. A way to cover this passage was through the utilization of methane: between the most diffused fuels it is the most efficient energy source due to its high-energy density and also lowest carbon per energy ratio [5].

Fuel	Emissions in g CO2/kWhPE
Wood	367.6
Lignite	398.7
Peat	366.5
Hard coal	338.2
Gasoline	263
Fuel oil	266.5
Diesel	266.5
Crude oil	263.9
Kerosene	263.9
Liquid petroleum gas	238.8
Natural Gas	200.8

Table 1: different CO2 emission per primary energy content of most important fossil fuels in the world.

The main methane source in the world is the Natural Gas (NG), but other cleaner sources, such as biomethane, and other methane production systems, such as methanation from green hydrogen and carbon dioxide, can replace the fossil source. Moreover, while its role as a reliable partner for clean energy transition was shared between different policy makers, NG demand in the last months had decreased due to Russia’s action in Europe: the decrease in NG stream between Russia and Europe can be estimated of 40% with respect to the first-half of the 2022, with many countries in EU that are not supplied at all (such as Netherlands, Poland, Denmark, Bulgaria, Finland, Lithuania and Estonia) while others that have partially cut the demand (Germany, France, Italy, Austria, Czech Republic and Latvia) [6]. In order to better understand terminology, IEA in its yearly “World Energy Outlook” publication takes into account three different scenarios:

- STEPS, Stated Policies Scenario, which reflects the current policy settings
- APS, Announced Pledges Scenario, which assumes that all climate commitments made by governments will be met in full and on time
- NZE, Net Zero Emissions by 2050 Scenario, which sets out the path to global energy sector to achieve net zero carbon dioxide emissions by 2050

Looking at the APS of EU after the Russian actions, it can be stated that there would be an acceleration of key measures (faster deployment of renewables and energy efficiency), which meet the GHG (Green House Gases) reduction targets much earlier than what REPowerEU Plan was expecting [7][8]. Other important short-term measures of the REPowerEU Plan include common purchase of gas, LNG and hydrogen and new energy partnerships with reliable suppliers. The last point has been a crucial part in the recent energy crisis of EU: in 2021 the most important countries in terms of NG utilization were Germany, Italy, France, Netherlands and Spain, respectively with a share of Russian NG of 46%, 41%, 20%, 36% and 11%: going in depth in this data, Netherlands share of gas in power and buildings sectors is the highest among the other markets, with 58% and 59%; Italy has similar values, respectively with 51% and 50% [6]. This shows the dependence of those country to methane, hence to Russia as energy supplier, due to their high share of gas. The ways to face this problem are new agreements with other NG producers, increase in efficiency of gas devices (both in building heat and power generation fields), substitute heat gas generation unit with heat pump systems (or other technologies that do not involve methane oxidation) and increase internal production of clean and sustainable methane, with biomethane or methanation plant fed by green hydrogen (produced through electrolyser supplied by electricity from renewable sources) [9]. These solutions are all going towards the energy security concept, which has many definition [10], but all of them have in common the diversification of energy supply. Economic growth is strictly correlated to energy consumption, and its dependence to the energy field has already been confirmed in recent history: in last years barrel of oil has been an indicator for global economy, in fact many global recessions have been associated with volatility in oil prices. Diversification can also be applied in internal energy production because having different ways to produce energy increase energy security: in renewable energy field it should be supported by storage system due to intrinsic unpredictability of the source in order to effectively improve supply management and network stability [11].

1.2 – Circular economy applied in CO₂ field

Circular economy (CE) is an economic system based on recycling material, making unused products of a certain process the source for another one [12].

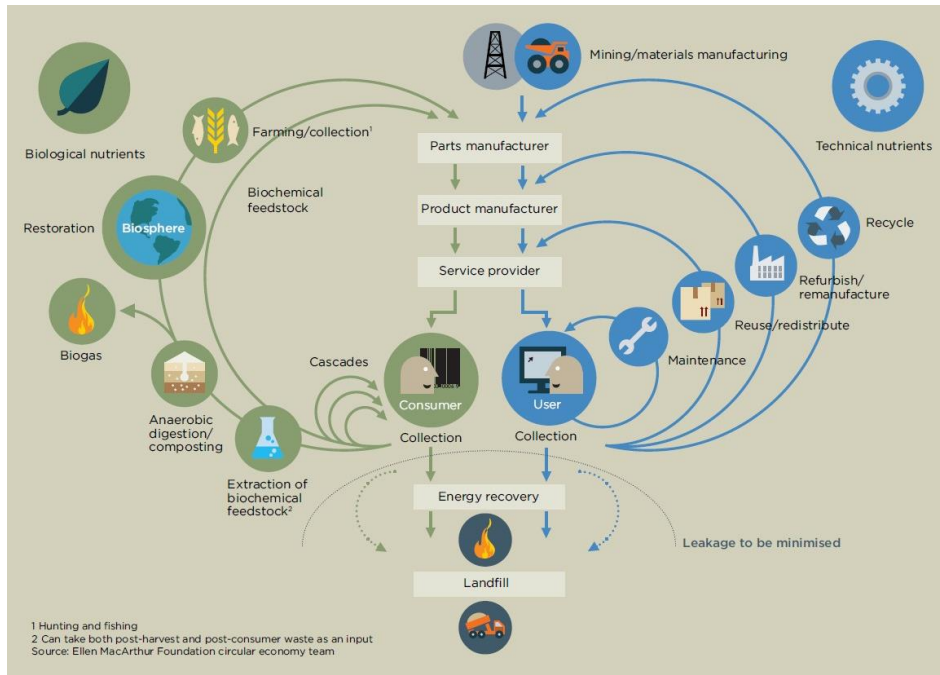


Figure 3: a scheme of circular economy, mainly divided in biological and technical nutrient [13].

The ideal scheme should not take into account any inlet or outlet arrows to the main circular part: economy system should be maintained by elements actually inside the circular economy, hence mining (as inlet side) and energy recovery or landfill (as outlet side) would not be represented. However, looking at figure 3, inlet materials, supplying new sustainable technologies or essential manufacturing industries, are needful in order to achieve main objectives given by policy makers; on the other side, some essential materials cannot be completely recycled, hence energy recovery followed by landfill are included as part of circular economy scheme that could be applied to a real case scenario; finally, growing world population will bring higher food demand, which could not coexist with the actual food production. The principles of the circular economy begin from the design of the product: all new materials should be planned to be part of a biological or technical cycle, in which can be reutilised after some maintenance or remanufactured activities or recycled with a lower energy demand and highest quality possible; technical items that can be utilized in many sectors or that can modulate its output should be preferred to the ones which can work only in the most efficient case, because modularity, versatility and adaptivity are the most important characteristics in a circular economic system; another important point in circular economy is based on renewable energy sources as main energy suppliers because of its ability to regenerate itself in less time with respect to the time spent to exploit it [13]. On the biological side, waste food is the main key to improve the system in a much more sustainable way: around one-third of all food produced is currently wasted rather than eaten (WFP, 2020), so decreasing waste food is necessary, while on the recycling side, the ability to reintroduce products material in the biosphere is the based idea [6].

From the point of view of carbon dioxide, it can be possible to apply the circular economy: in this case it is called circular carbon economy (CCE) [14]. CCE is based on the same concepts of CE, which can be summarized by reduction, re utilization and recycle, but it also takes into account the removal of carbon dioxide. Going in depth, reduction is strictly related to energy efficiency and new energy supply installation, that can reduce the flow of carbon into the system (i.e. nuclear and renewables), but do not completely avoid carbon emission due to manufacture, construction and installation phases; re utilization is based on storing a CO₂ stream that did not have a chemical reaction and use it again in a process; recycling is based on chemical reactions that involves CO₂ as a reactant which give a product that can be saleable; removal can be considered as the stage before both reutilization and recycling, in which carbon dioxide is stored in some empty volume or captured in natural sinks.

CO₂ can be utilized in many fields, which can be divided into chemicals and durable materials, mineral carbonation and construction materials, biological algae cultivation and enzymatic conversion [15] and enhanced oil recovery. CO₂ to chemicals and durable materials is a category which can include production of urea, inorganic carbonates, polyurethane, polycarbonates and salicylic acid, but also methanol, methane and formic acid through hydrogenation process using various catalysts [16]. Mineral carbonation could be another way to store carbon dioxide inside pores of different materials, most of them composed by calcium or magnesium silicates [17], while for what concerns building materials, CO₂ gas acts as a curing agent, yielding a binding matrix, to improve performance of CO₂-based materials [18] and also leading the way to a more sustainable path for the concrete industry by storing part of carbon dioxide that would be emitted in atmosphere. In a similar way to natural photosynthesis processes, many types of algae can convert CO₂ into different hydrocarbons or lipids [19], while for enzymatic conversion the most interesting reactions involve cyanobacteria, which has great potential in terms of biofuel generation [20]. Another kind of utilization is related to enhanced oil recovery, in which CO₂ is injected into oil reservoir: nowadays carbon dioxide is the most efficient injected gas for this kind of purposes from the economic and environmental point of view [21].

1.3 – Thesis objectives

After a general introduction about carbon dioxide emissions, European policies and investments against climate change, new energy plans after Russia invasion and a description of circular economy, a technical review about carbon capture technologies for biogas application is carried out. This is followed by a in-depth study about membranes for gas mixture separation. This section is divided by material composition, transport mechanisms and technological limits. Then a Matrimid membrane and new polymeric membranes are tested with methane and carbon dioxide. While Matrimid has well-known characteristics, three different polymeric membranes were provided by chemical department of UNITO in order to evaluate their performances in gas separation: these are PES-WC, PES-WC with cyclodextrin nanosponge and PEEK-WC. In order to evaluate permeabilities and selectivities of these membranes, it was used an

experimental test bench in Environmental Park (Turin, Italy) at the CO2 Circle Lab (CCL). Tests were performed both in closed volume (evaluation of the change in pressure) and open volume (direct gas flux measurement) at isothermal conditions.

2 – Biomethane as substitute of fossil methane

Most important arguments which took the side of NG concerned its cleanliness with respect to other fossil fuels and its ability to be a good substitute for coal and oil, but with both the increasing climate change and Russia’s action in Europe NG availability is expected to decrease, while on the other hand its cost is expected to increase because of new contracts at higher prices with other suppliers. Looking outside Europe, in USA its recent Inflation Reduction Act should make renewable energy sources much more relevant in the power sector, increasing heat pumps installation for buildings heating; price-sensitive emerging markets (and in general developing economies) prefer not to switch from coal to gas due to its costs increase, but in Asia many countries have stipulated long-term gas imports contracts which provide a partial protection from volatile gas prices [6].

2.1 – NG trends in different scenarios

	HYSTORICAL DATA		STEPS		APS		NZE	
	2010	2021	2030	2050	2030	2050	2030	2050
Natural gas demand (bcme)	3329	4213	4372	4357	3874	2661	3268	1159
Power	1345	1633	1590	1469	1422	880	1177	119
Industry	701	882	1003	1116	891	644	802	213
Buildings	757	886	890	852	737	372	486	0
Transport	108	147	159	172	126	58	99	12
Low emission H ₂ products and other	418	665	730	748	698	707	704	815

Table 2: Natural gas demand in different sectors and scenarios [6].

IEA in the three main paths analyses the change in gas demand in the different fields. In the Stated Policies Scenario (STEPS) NG stays almost the same between 2021 and 2030 with an increase just of 0.4%, while between 2010 and 2021 there were an increase of 2.2%, in particular in the industry field in which an increase of almost 60% between 2010 and 2050 can be noted; however, total demand reaches a kind of plateau between 2030 and 2050 because in the heating space field technologies based on electricity are preferred (heating pumps or electric heaters), while for domestic heat water solar thermal heating takes the place of gas heater. In the Announced Pledges Scenario (APS) global NG demand reaches a peak in nowadays period, with a decrease of 8% and 36.8% in 2030 and 2050 with respect to 2021 data; in particular an important change in the field of transport is expected, with a decrease of 60.5% in 2050 with respect to the values registered in 2021, but also in buildings with a decrease of 58%. Similar to APS scenario, in Net Zero Carbon total NG demand reaches the peak in 2021, with a significant reduction in the buildings and transport with almost zero gas demand. Most important direct use of methane is in non-combustion sectors such as chemicals with 190 bcm in 2050, while for what concerns electricity generation 100 bcm is burnt in power plant with carbon and capture storage systems [6].

While the previous data are related to world trend, EU plans are summarized in the REPowerEU Plan [7], which is mainly based on the “Fit for 55” proposals. In order to reduce the dependency on Russian fossil fuel and accelerate the energy transition, REPowerEU Plan set its principle in four different points:

- Save energy
- Diversify supplies
- Quickly substitute fossil fuels by accelerating Europe’s clean energy transition
- Smartly combine investments and reforms

From the energy savings point of view, it is the quickest and cheapest action in order to face this energy crisis. EU proposals would lower gas consumption by 30% by 2030, which is equal to 116 bcm. In order to substitute the NG demand within 2030, an increase in renewables to a 45% of share, energy efficiency reaches 13% share in 2030, increase in bio-methane production, renewable hydrogen use reaches 20 Mt.

2.2 – Biogas and biomethane in EU

While methane from fossil sources is expected to decrease, a scaling up of biogas and biomethane is planned, with an increase in production to 35 bcm by 2030 and estimated investment of 37 billion euro over the period. These investments are justified by the fact that biomethane, which is a product of biogas, could resolve two critical challenges, that are dealing with the increase amount of organic waste that is produced and reducing global greenhouse gas (GHG) emissions. Turning organic waste into a source of energy is in totally accordance with carbon circular economy principles; moreover, when biogas is upgraded into biomethane, it is indistinguishable with respect to NG, hence it can be compressed, transported and burnt with the same technologies that have been used. There are many actions taken by the REPowerEU Communication of March 2022 [22].

In the Area of promoting sustainable production and use of biogas and biomethane and its injection into the gas grid, an industrial partnership should be created, in which strategic discussion among key stakeholders would be essential in order to better support the production and use of biogas and biomethane: main discussion would focus on identifying and developing the best practices in policy making, in which infrastructure development and financing and promotion would be the most relevant; moreover, partnership should also constantly communicate and create synergies with different EU projects in this field, such as the European Technology and Innovation Platform Bioenergy (ETIP Bioenergy), the SET Plan Action 8 Integrated Workgroup on Bioenergy and Renewable Fuels (IWG 8) and other international cooperation. Another development could be the definition of national strategies towards the objective of 2030 and 2050: they should focus on most sustainable paths, based on waste based production (such as agriculture and agro-industry waste residues, forest and forest-industry waste food industry waste, industrial waste water and domestic organic waste) and evaluate the

potential of other renewable sources coming from sequential or cover cropping, following the related directive [23]; national strategies should take into account a standardization of market regulation about production and injection of biogas and biomethane.

Most important costs in biomethane field are the ones related to upgrading, grid connection and grid injection. The content of existing promotion plans at national level for electricity production from biogas should also be reviewed to focus on support for biogas upgrading. In this context, the benefits of developing take-off agreement tools or other incentives, to ensure that there are long-term benefits for biogas plants currently providing electricity to be converted into biomethane plants as well as for new biomethane investments, should be considered [22].

For what concerns the adoption and adjustment of existing and the deployment of new infrastructure, an analysis should be carried out by the distribution system operators, in coordination with transmission system operators and in general national regulatory authorities, establishing a regional map with the highest potential for biogas and biomethane from the available and admitted sources [7] [8]. When looking at cross-border flows of biomethane, the most important problem is related to the uncoordinated application of existing gas quality standards across borders [24].

Research and Development fields should be supported by innovative technologies for the production of sustainable biogas and biomethane, primarily based on gasification of biogenic residues and wastes from all sectors and industries, biogenic carbon dioxide effluents and waste, organic part of industrial waste waters and municipal sludge, with a particular focus on technological efficiency progress and cost effectiveness of small-scale solutions.

Generally, possibilities to produce biomethane in the world are widely distributed around the world and the availability of sustainable feedstocks for these purposes can increase of 40%. Nowadays production of biogas is strictly related to power and heat generation because of its easier and cheaper application with respect to biomethane production, but next years the upgrading technologies are expected to increase, hence much more green methane should be injected in national grid [25]. Looking at the *figure 4*, the statement above can be confirmed: in fact, energy from biogas remained almost constant between 2016 and 2021, while an increase in biomethane production through upgrading process can be observed since 2011, with a production of 0.5 bcm, until 2021, with a production of 3.5 bcm [26]. This is enhanced by the fact that biomethane is a better product with respect to biogas due to its wider application: biogas is limited to heat and power generation, while biomethane is a much more versatile energy carrier since can be used in other sectors, such as transport an industry.

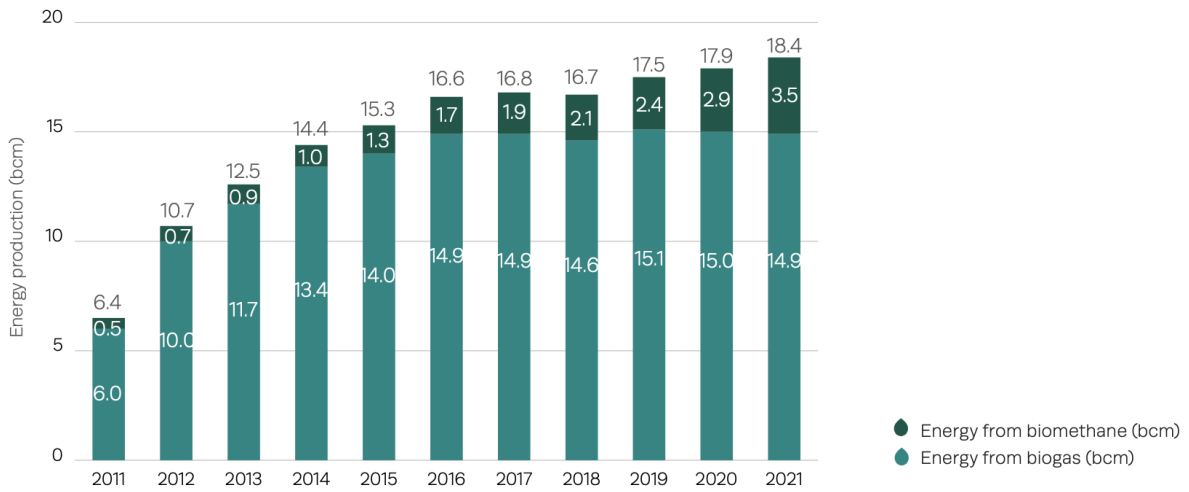


Figure 4: biogas and biomethane production in EU in the last years [26].

Looking at the *figure 5*, REPowerEU Plan the biogas and biomethane sectors combined can increase production from 18.4 bcm to 35 bcm in 2030. Looking forward, by 2050 production is expected to be between 95 bcm and 167 bcm. The potential production range calculated to be reachable by 2050 (95-167 bcm) is significant, as the 2021 EU gas consumption was 412 bcm. The 2050 production potentials thus represent 23-41% of the gas consumption of the EU in 2021. Assuming a reduced total gas demand in 2050 of 271 bcm, it is estimated that biomethane will be able to cover 35 – 62% of the gas demand by 2050.

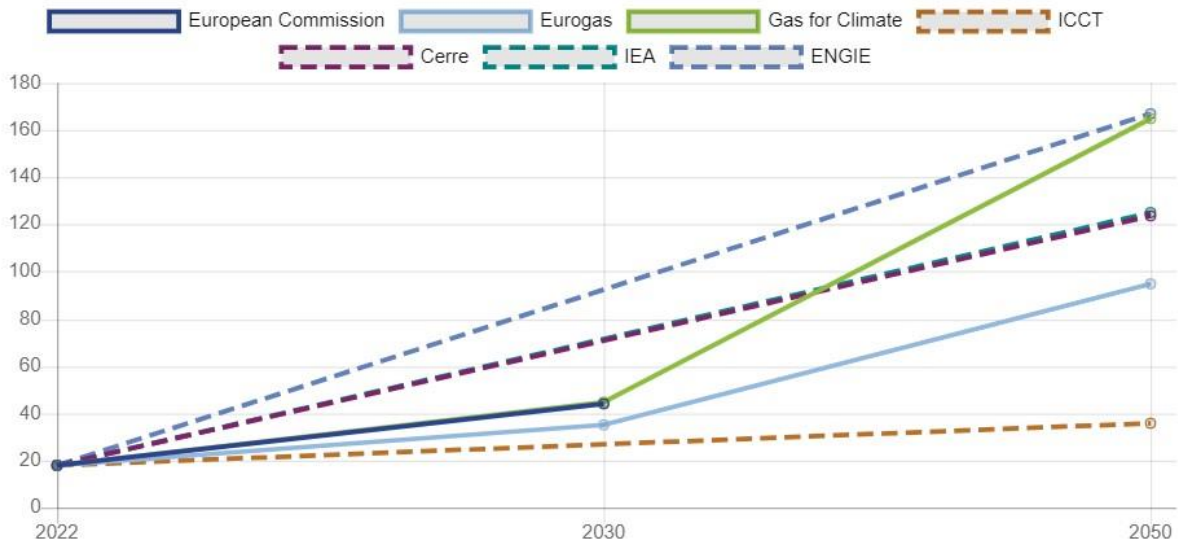


Figure 5: possible trend scenario of biogas and biomethane production from different sources in bcm[26].

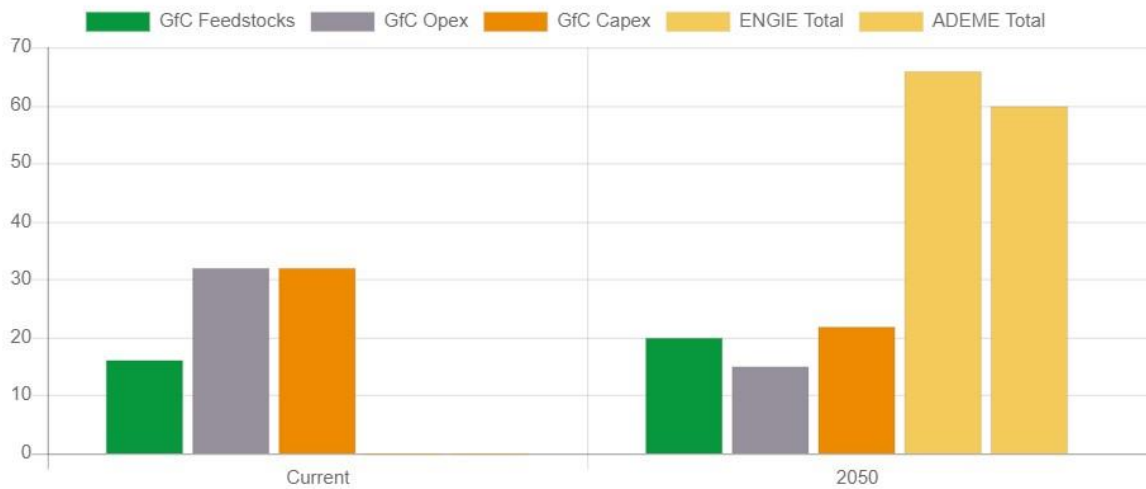


Figure 6: costs of biogas production calculated from different sources [26]

The current trends show that biomethane production costs are already significantly below the expected average TTF gas price for 2022 (80 €/MWh as opposed to 134 €/MWh), hence speeding up biomethane production and accelerating the clean energy transition in general are of high importance to stabilize gas prices and ensure energy security. Additionally, phasing out fossil energy with biogas or biomethane also means the replacement of a product that is otherwise almost completely produced abroad. As biogas and biomethane are locally produced, using local organic waste streams, local jobs are created.

3 – Biomethane upgrade systems

3.1 – Biogas composition, production and cleaning processes

The growing of biogas through biological fermentation is considered a solution to the energy crisis and GHG problem. Biogas can have different composition based on the main organic source: it can be summarized in the following table [27].

Composition	NG	Biogas			
		Waste water	Food waste	Animal waste	Landfill
Methane [% vol.]	80 - 100	50 - 60	50 - 70	45 - 60	40 - 55
Carbon dioxide [% vol.]	< 3	30 - 40	25 - 45	35 - 50	35 - 50
Nitrogen [% vol.]	< 3	< 4	< 4	< 4	< 20
Oxygen [% vol.]	< 0.2	< 1	< 1	< 1	< 2
H ₂ S [ppm]	< 0.1	< 400	< 10000	< 300	< 200
Non H ₂ S sulfur [ppm]	< 10	< 1	< 1000	< 30	< 30
Halogens [ppm]	< 0.1	< 0.2	< 0.2	< 0.2	< 100
Moisture [%]	< 0.02	3	3	3	3

Table 3: compare between NG and different biogas composition [27].

Most important sources are:

- Landfill: if mixed with oxygen can create an explosive mixture, it is really important to isolate from comburent, better collect it and use for energetic purposes
- Organic fraction from municipal solid waste
- Sewage sludge: it is a by-product of wastewater treatment, due to its concentration of heavy metals the digestate cannot always be as soil conditioner (the alternative is to burn it in a waste incinerator); decrease in volume of digestion process reduce the disposing costs and problem
- Manure: normally stored on farms many months before its utilization, which releases GHG (methane, ammonia and carbon dioxide) due to the presence of digesting micro-organism inside.
- Energy crops: dedicated crops planted on agricultural land (typically maize or sweet sorghum); it is the driest matter per hectare between all of these sources and it has high conversion efficiency.

Biogas production occurs by anaerobic digestion, which is a series of processes in which microbes break down biodegradable material without the use of oxygen. Anaerobic digestion is carried out by a variety of microorganisms, such as bacteria that produce acetic acid (acetogens) and methanogens (bacteria that produce methane, methanogens) [28]. These organisms consume the primary feedstock, which is transformed by a variety of processes into

intermediate molecules like sugars, hydrogen, and acetic acid before being transformed into biogas. It is divided into four phases:

1. Hydrolysis: Anaerobic bacteria in this phase break down non-dissolved substances like proteins, lipids and carbohydrates into monomers (water-soluble bits). When water is involved in a chemical reaction, covalent connections are broken. The hydrolysis of carbohydrates happens in a matter of hours, while that of proteins and lipids in a matter of days. Lignocellulose and lignin are broken down slowly and partially.

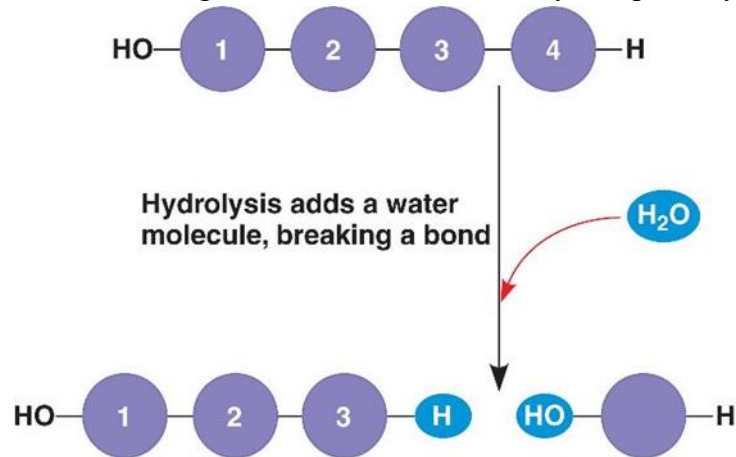


Figure 7: breaking bonds phenomena by hydrolysis.

2. Acidogenic Phase: Different anaerobic bacteria metabolise the monomers created during the hydrolytic phase and convert them into short-chain organic acids, such as C1-C5 molecules.

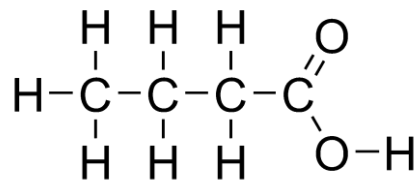


Figure 8: butyric acid.

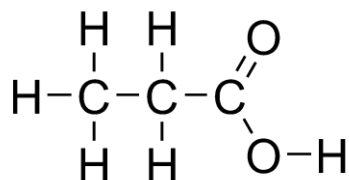


Figure 9: propionic acid.

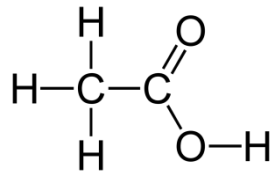
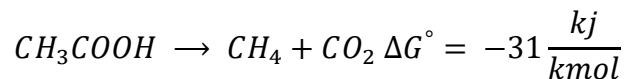


Figure 10: acetic acid.

3. Acetogenic Phase: the acetogenic bacteria are primarily responsible for producing H_2 , CO_2 , and acetate when the hydrogen partial pressure is low. Most commonly, ethanol and butyric, caproic, propionic, and valeric acids are generated when the hydrogen partial pressure is higher. Bacteria involved in acetogenic phase need products from the acidogenic ones.
4. Methanogenic phase: methane generation takes place under strictly anaerobic conditions, hence without the presence of oxygen. Main chemical reaction is the following



Before biogas is upgraded to biomethane, a cleaning process is needed in order to remove all impurities (water, siloxanes and hydrogen sulphide) [29]: these gases need to be eliminated since they could either reduce the calorific value of biogas or have a greater detrimental effect by being harmful to both people and other living things. Additionally, siloxanes produce issues in gas combustion motors due to the production of glassy microcrystalline silica, while H_2S and NH_3 are exceedingly corrosive, ruining valves, tubes, monitoring equipment, gas motors, etc.

Desulfurization processes remove H_2S and its products from the raw biogas. The most important processes are [30]:

- In situ H_2S Precipitation: by using iron salts, a reaction between Fe and S is forced, and the resultant FeS is removed from the system (it can be oxidized with atmospheric oxygen in order to become a fertilizer)
- Adsorption: a chemical reaction between Fe_2O_3 , $Fe(OH)_3$ or ZnO , H_2S and oxygen is performed in regenerative modules
- Membrane separation: selective permeability under different pressure between feed side and permeate side is done in order to separate both gas and liquid from the raw biogas
- H_2S absorption: water with chemical reagents performs physical absorption and transform H_2S into elemental sulphur or metal sulphides; it also separates CO_2 from the raw biogas.

For what concerns biogas drying process, water can be removed by physical separation (condensation) and chemical drying (adsorption). For what concerns physical separation,

biogas is cooled at atmospheric pressure to produce condensation, which is followed by the separation of the condensed water droplets using demisters, cyclones or water traps. Due to operational issues brought on by water freezing at the heat exchanger's surface, these configurations constitute the most basic but least effective water separation technique, which can only lower the methane dew point to 0.5°C. In the chemical drying, the process primarily involves the absorption of water into glycol, a drying agent with a binding component that can lower the dew point from -5°C to -15°C and regenerate at 200°C. With the use of this technology, oil and dust particles can be eliminated at the same time as water is absorbed. However, because of the energy-intensive solvent regeneration and its somewhat high operating pressures, it has substantial operating and investment expenses [31].

After a brief review of cleaning biogas methods, biogas can be upgraded into biomethane by separate the carbon dioxide from the CO₂/CH₄ stream. Most important technologies in biogas upgrade are represented in *figure 11*. There are analysed in this chapter, except for membrane separation ones, which are examined in the next chapter.

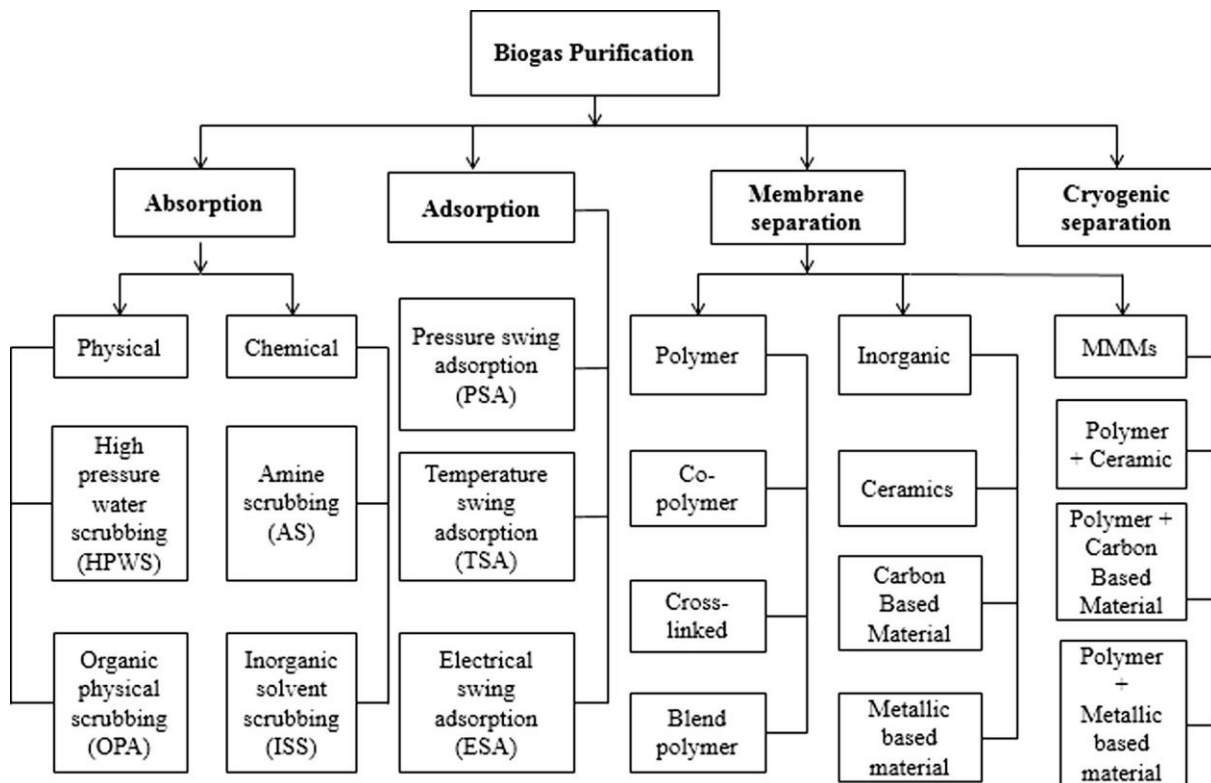


Figure 11: a scheme of different technologies for biogas purification [32].

3.2 – Absorption

The varying solubilities of CO₂ and CH₄ in various solvents are used in physical absorption. Thus, the two gases can be separated by choosing a solvent that has a high solubility for CO₂ but it is non absorbing with respect to CH₄. Water in high pressure water scrubbing and organic

solvents in organic physical scrubbing are analysed as physical absorption, while amine scrubbing and inorganic solvent scrubbing as chemical absorption.

3.2.1 – High pressure water scrubbing (HPWS)

Water is a selective absorbent that is frequently employed in the industrial scale upgrading of biogas. Due to their reduced sensitivity to biogas pollutants, water scrubbing systems currently account for 41% of the global market for biogas upgrading.

At 25 °C, CH₄ is 26 times less soluble than CO₂. Additionally, these molecules are separated using the various binding energies between the nonpolar CH₄ and the polar CO₂ or H₂S. Since H₂S is more soluble in water than CO₂, it is theoretically possible to remove H₂S together with CO₂. However, it is preferable to separate the H₂S before the CO₂ due to a number of benefits, namely the fact that getting rid of the dissolved H₂S reduces operational issues like motor corrosion and odour annoyance issues. When the gas stream contains a high percentage of H₂S, pre-removing the H₂S is a necessary step in water scrubbing processes like PSA [33].

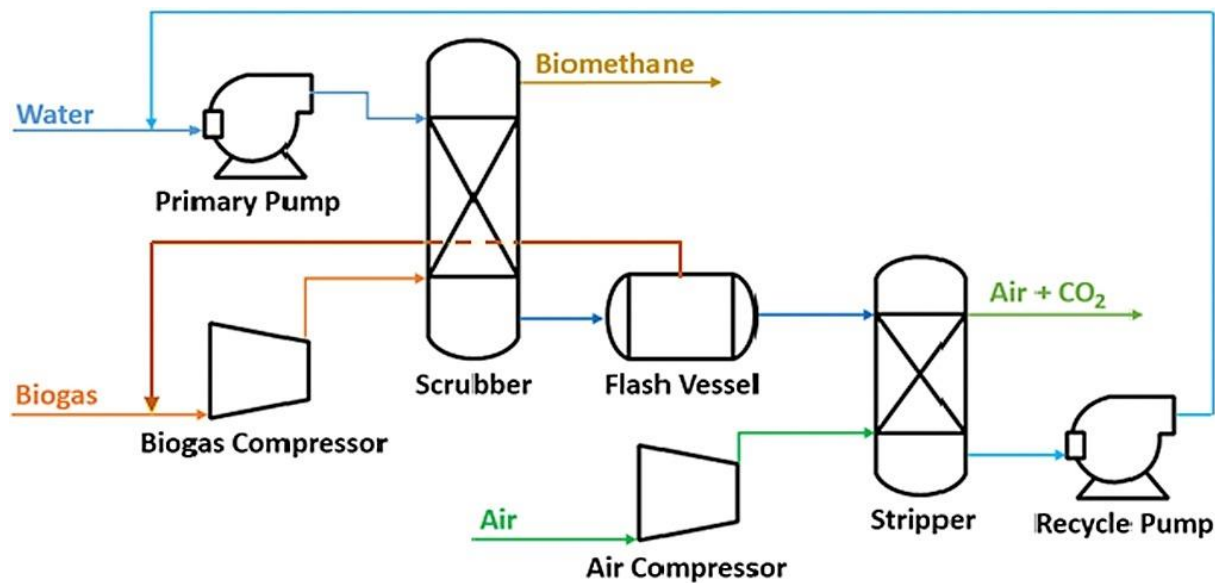


Figure 12: high pressure water scrubbing scheme [34].

There are currently two approaches of reusing water: when water is collected from sewage treatment plants, the first method, known as "single pass scrubbing" is used; the second technique, referred to as "regenerative absorption," involves decompressing (often accomplished by air stripping) water in a desorption column to regenerate it at atmospheric pressure, resulting in the elimination of CO₂ and H₂S. Due to the significant amounts of water needed, the regeneration process is crucial for both the economic viability and environmental sustainability of this biogas upgrading technology [29]. From an economical point of view, biogas and air compressor together with the scrubbing column are the most expensive elements in this kind of plant [34].

3.2.2 – Organic physical scrubbing

Similarly to high pressure water, carbon dioxide in the biogas is absorbed in an organic solvent during organic and physical cleaning. Main difference is that the amount of solvent that must be recirculated in the process is decreased because the carbon dioxide in the solvent has a greater saltiness, which means that also pumping systems require less energy involved. Another difference is referred to diameter of columns: since lower flow of the organic solvent is needed the columns' diameters are smaller. Main drawback is that, in order to correctly work, it has to be heated before desorption and chilled before absorption. The biogas is cooled and compressed to 7-8 bar before being injected at roughly 20°C into the bottom of the absorption column. Prior to be sent to the gas grid or the fueling station, the improved biogas is dried and the carbon dioxide is absorbed by the organic solvent. Before entering the desorption column, the organic solvent is heated up to a further 40 °C to renew it. The pressure is reduced to 1 bar as the solvent is pumped into the column's top. The absorption column's top receives an injection of the regenerate solvent. Although the CO₂ separation efficiency of this procedure is superior to that of water scrubbing, solvent regeneration consumes more energy. Additionally, the price of organic solvents is much greater than the price of water [35].

3.2.3 – Amine scrubbing

In general, chemical absorption involves reversible reaction between absorbed substances and solvent. Diethanolamine (DEA), monoethanolamine (MEA), and methyl diethanolamine (MDEA) are the three amines that are most frequently employed as solvents for the removal of acidic gases (CO₂ and H₂S). An amine scrubber system typically comprises of an absorber where the CO₂ is absorbed from the biogas and a stripper where the CO₂ is heated under decreased pressure to remove it from the waste amine solution [32]. The amine solution is fed to the top of the column to create a countercurrent flow contact as the raw biogas enters the absorber from the bottom. The amine solution reacts with the carbon dioxide of the biogas stream, which is then absorbed. This exothermic process raises the absorber's temperature from 30±10°C to 55±10°C. However, in amine scrubbing (AS), the reaction rate between the CO₂ and the amine solution rises with rising temperature, resulting in increased absorption of CO₂. The column's top is where the product gas (CH₄) leaves. The absorber operates at 1-2 bars of pressure. After passing through the heat exchanger and being pushed to the top of the stripper column, where it is linked to the steam and CO₂ is discharged, the liquid from the bottom of the absorber is released. A reboiler at 120–150 °C is included in the stripper column's bottom section, where amine solution is heated. The reboiler regenerates the amine solution while providing the heat of reaction for the release of CO₂ from the used amine solution. Low operational costs but high investment costs are used to produce highly concentrated CH₄ that is > 99% gas; also, high heat power is needed to regenerate the amine solution [36].

3.2.4 – Inorganic solvent scrubbing

Typically, an aqueous solution of alkaline salts such sodium, potassium, ammonium, and calcium hydroxides is used in inorganic solvent scrubbing (ISS). In this alkaline solution, agitation aids in the absorption of CO₂. The solvent's turbulence and the amount of time that biogas and liquid are in touch with one another both speed up the diffusion of CO₂ [32].

3.3 – Adsorption

In this separation technique, gas is separated from the gas mixture during the adsorption process when it comes into contact with porous particles that may adsorb the gas due to its surface affinity (e.g., comparable chemical groups). The adsorption procedures are regarded as sophisticated separation techniques. The poor efficiency of the gas separation process is one of the current limits of research that tries to reduce the costs of these operations. The requirement for huge quantities of energy to operate the process, or the unfavourable energy balance, is another barrier to the development of adsorption technology [37].

3.3.1 – Pressure swing adsorption

The dry technique of PSA for biogas upgrading is based on the selective adsorption of CO₂ over CH₄ onto porous solid adsorbents materials that are packed in columns. Since the adsorbents in PSA can be irreparably damaged by H₂S, pre-treatment targets for H₂S removal are necessary before employing PSA to remove CO₂ because the adsorption material used for biogas upgrading adsorbs H₂S irreversibly [38]. The PSA process, in its basic form, entails two main steps:

1. the adsorption step, in which the solid adsorbent adsorbs the strongly adsorbable component until it reaches saturation
2. the desorption step, in which the previously adsorbed component is released from the adsorbent and the adsorbent is renewed and ready for the next iterative cycle.

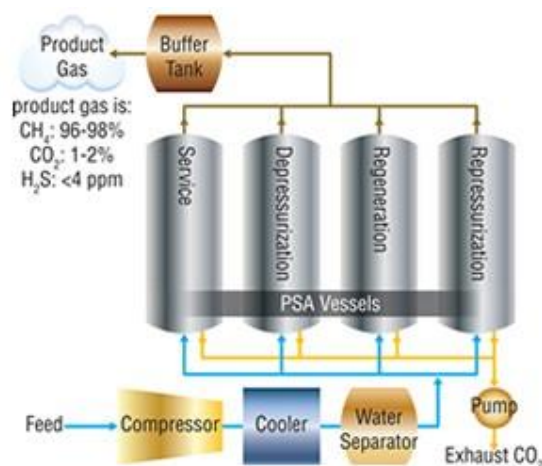


Figure 13: a biogas upgrading systems with PSA technology [39].

Zeolite, activated carbon, activated charcoal, silica gel, and synthetic resins are the most frequently utilised adsorbents. The percentage of CH₄ recovered is around 96%–98%, with methane losses of 2%–4%. However, despite the equipment supplier's assertion that the losses should be under 2%, 10% to 12% of the methane in the two PSA facilities was lost, according to an examination. In general, with greater purity standards, more CH₄ is lost. This technology is useful since it takes less energy and capital investment, has little capital requirements, and is safe and easy to use.

3.3.2 – Temperature swing adsorption

Due to higher CO₂ capacities and lower material heat capacities of sorbent material compared to aqueous solvent, continuous temperature swing adsorption (TSA), which involves the use of appropriate adsorbent material, has been proposed as an upgradeable alternative to scrubbing methods. Lower temperatures are used for adsorption whereas higher temperatures are used for desorption. Temperature swing adsorption makes it possible to regulate the process using moderate temperatures and air pressure, but it's still crucial to maintain proper control over the temperatures used for adsorption and desorption. A departure from the norm might result in reduced adsorption activity or poor desorption performance [40]. On the one hand, the TSA process's exothermic CO₂ adsorption onto amine sorbents necessitates active cooling of the sorbent substance in order to maintain the adsorption temperature. On the other hand, the endothermic desorption process requires the same amount of energy in order to keep the desorption temperature constant. In terms of heat fluxes, which provide the thermodynamic driving power for the separation process, these cooling and heating needs have an impact on the overall efficiency and economics of a TSA process. Heat transmission therefore demands high rates between adsorbent material and internal heat exchanger surfaces and is one of the most significant influencing factors.

3.3.3 – Electrical swing adsorption

The slow and indirect heating of the adsorbent, which decreases process efficiency, is one of the primary problems of conventional TSA procedures. This results in a lengthy cycle time. Therefore, electric swing adsorption (ESA), which uses the Joule (resistive) heating method to directly heat the adsorbent, may be a preferable option. As the heat is given directly to the adsorbent using this approach, the heating step is more effective. Adsorbent heating may happen considerably more quickly, which might result in a quick TSA system. Another benefit is the possibility of greater purities due to the purge gas's independence from the heat flow, which is employed to remove the desorbing species [41]. Numerous research on ESA in recent years have emphasised CO₂ collection from exhaust gases (CO₂ concentration between 3.5% and 15%). Usually, a 4-step procedure is applied:

1. Adsorption occurs when the feed gas is passed over the adsorbent
2. Electrification to heat up
3. Purge stage with an inert gas
4. Cooling the adsorbent to the initial temperature

One of the biggest ESA-related restrictions when considering CO₂ collection is the demand for a conductive adsorbent. The electrical characteristics of activated carbon are frequently employed, but they are also associated with a decreased adsorption capacity, particularly at lower partial pressures. The heating process needs to be effective and uniform, which is another essential component of ESA. Inhomogeneous electrical conduction and heating are seen when utilising particulate carbon adsorbents. Therefore, as they provide an uninterrupted channel for the electrons across the structure, preventing the creation of hot spots, structural adsorbents such monoliths, carbon fibres, or hollow fibres have been preferred.

3.4 – Cryogenic separation

H₂O, H₂S, CO₂, and CH₄ may be separated out of biogas by using various temperatures for liquefaction and solidification. According to their different boiling points, different gases must be separated via cryogenic separation, which involves a progressive drop in temperature [42]. Through a series of periodic temperature drops, the cryogenic process produces liquefied biomethane that is similar to liquefied natural gas (LNG) by separating liquefied CH₄ from CO₂ and other components of biogas. The technique handles at very low temperatures and high pressures. Cryogenic biogas upgrading is started by compressing the gas and cooling it to -25°C. Then, the H₂S, siloxanes, halogens, and water are eliminated. The temperature is then further lowered to -55 °C, when the majority of the CO₂ is dissolved, and finally to -85 °C as the last phase, where the residual CO₂ transforms into form. The biomethane produced may attain purity of over 97% and methane losses of less than 2% with the cryogenic upgrade. The most crucial step in the cryogenic process is the low-temperature requirement. Low temperatures aid in removing CO₂ from biogas with great efficiency. Rejecting the use of

chemicals in the system and employing CO₂ as a byproduct are two benefits of cryogenic methods for upgrading biogas. The main issue with the system for producing and selling upgraded cryogenic biogas is how much energy it requires to operate a variety of machinery, including compressors, generators, distillation columns and heat exchangers.

4 – Membranes for CO₂ separation

Most important technologies installed for CO₂ and CH₄ separation are the ones that involve the absorption process; although it is fully developed, the phase dispersion that takes place during the process usually leads to issues such as flooding, excessive loading, weeping, foaming, and entrainment. Additionally, those traditional procedures often need a lot more expensive and intricate equipment, as well as more energy [43] [44].

As an alternative, membrane separation technology has demonstrated promising properties and, as a result, it has drawn increasing attention from the scientific community with research focused on CO₂ capture: energy efficiency, straightforward process design, simplicity in scaling up, ease of building modules, and small environmental impact are the most important strengths [45]. Gas separation research utilising membranes have advanced significantly over time in terms of membrane production, enhancement of the chemical and physical characteristics of the membrane, process design, and module layout. It is important to keep in mind, though, that while membrane technology seems promising for gas separation, it is challenging to sustain the membrane performance over an extended period of time. One of the major obstacles to membranes' potential applications in industrial practise is that most membranes lack the robustness to withstand real-world industrial settings and soon break. However, membrane-based technology has emerged as a competitive separation method and a successful CO₂/CH₄ separation instrument.

The technology's fundamental tenet is dependent on the selective permeability capabilities of membranes, which enable the separation of the biogas components. While CH₄ is held on the intake side of the membrane for biogas upgrading, CO₂ passes through to the permeate side. Given this basic working principle, membranes can be mainly divided by the material they are made of: they can be polymeric, inorganic or mixed matrix membranes. Another way to distinguish membranes is by the transport: for dense or non porous membranes Fick's law is the main mechanism, while Knudsen is mainly referred for porous membranes. Finally, a section about main technology limits is carried out.

4.1 – Materials for membrane technologies

4.1.1 – Polymeric membranes

The open porous membranes used in microfiltration/ultrafiltration and the dense nonporous membranes used in gas separation and pervaporation will be categorised. The distinction in requirements when using polymeric materials as membranes is the basis for this categorization. The choice of material for porous microfiltration/ultrafiltration membranes is primarily influenced by processing needs (membrane manufacturing), fouling propensity, and chemical and thermal stability of the membrane. The selection of the material directly affects the performance of the membrane for the second class of polymers used for gas separation and pervaporation (selectivity and flux) [46].

Another way to distinguish polymeric membranes is by the glass transition temperature, T_g . The glass transition temperature is a temperature in which the structure of the polymer changes: above T_g the polymer has a rubber-like behaviour, while below T_g it has a rigid and fragile behaviour. They can be categorised as glassy or rubbery polymers depending on their thermodynamic state at room temperature (whether their glass transition temperature, T_g , is at or above the atmospheric value). Rubbers are equilibrium phases that are thermodynamically equivalent to liquids and are distinguished by having high values of the diffusion coefficients for all gaseous species because of the mobility of the molecular chains and the high free volume. As a result, the thermodynamic factor S , or the gas solubility, mostly controls their selectivity. Glassy polymers, on the other hand, are locked in non-equilibrium structures and exhibit a stiff polymeric lattice due to the kinetic barrier of chain relaxation [47]. For the so-called "structural recovery," the glassy state may be thought of as a kind of non-equilibrium condition that is leaning towards the rubbery state. The transition temperature is the defining moment for these changes in amorphous polymers, whose chain is solid but not organised geometrically.

Another important variable in membranes is the free volume. It is defined as the space between polymer chains that allows gas to permeate through; it can be generated by a flaw in the packing of the polymer during its production, but it can also be created by motion of a molecular chain on a transient state. It should be mentioned that polymers with stiff chains that belong to the glassy state have higher free volume than rubbery state polymers. In particular, the more pores there are, the more acceptable motion there is as a result of the greater temperature. In general, changes in mechanical characteristics and heat capacity occur together with the shift from a glassy state to a rubbery one [48].

4.1.1.1 – Porous membrane (microfiltration and ultrafiltration)

Fixed holes in the range of 0.1 – 10 μm for microfiltration and 2 - 100 nm for ultrafiltration are present in porous membranes. The size of the pores is the primary factor in determining selectivity, but the material choice also has an impact on phenomena like adsorption and chemical stability under conditions of real application and membrane cleaning. This suggests that the chemical and thermal characteristics of the material are also important factors in determining the needs for the polymeric material, in addition to flux and selectivity. Flux reduction as a result of concentration polarisation and fouling is the primary issue with ultrafiltration and microfiltration. Consequently, the selection of the material is mostly centred on how to clean the membranes after fouling and avoid fouling. The polymeric material's chemical and thermal resistance are also crucial in applications involving non-aqueous mixes or high temperatures.

Microfiltration membranes can be prepared using a variety of methods, including sintering, stretching, track-etching and phase inversion. Except in the case of phase inversion, these methods are not often employed to manufacture ultrafiltration membranes since the pore sizes achieved are only in the microfiltration range. Consequently, the polymers utilised for

ultrafiltration and microfiltration membranes are not, "a priori," the same. Most important polymers used for microfiltration membranes are:

- polycarbonate
- poly(vinylidene-fluoride)
- polytetrafluoroethylene
- polypropylene
- polyamide
- cellulose-esters
- polysulfone
- poly(ether-imide)
- polyetheretherketone

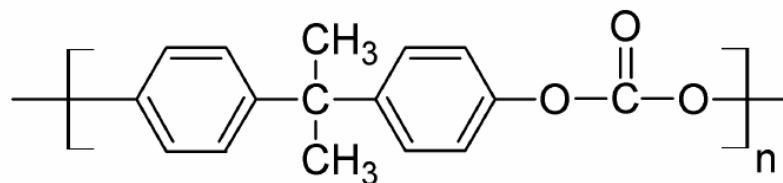


Figure 14: chemical structure of polycarbonate [46].

It is possible to create a unique sort of microfiltration membrane by track-etching different polymeric films. This is a common usage for polycarbonate (chemical structure in figure 14) due to its excellent mechanical qualities.

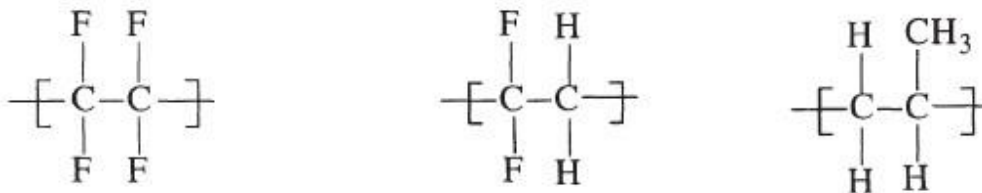


Figure 15: chemical structure of polytetrafluoroethylene, polyvinylidene fluoride and polypropylene [46].

The three polymers in figure 15 show good to outstanding chemical and thermal stability. Because of their hydrophobic characteristics, these membranes must be pre-wetted before being utilised in watery solutions (e.g. by the use of ethanol). Additionally, as they are not contacted by water or other liquids with a high surface tension, they may be employed in membrane distillation.

For what concerns ultrafiltration membrane, the most diffused are:

- polysulfone/poly(ether sulfone)

- poly acrylonitrile
- cellulose esters
- polyimide/poly(ether imide)
- polyamide (aliphatic)
- poly(vinylidene fluoride)
- polyetheretherketone

Since microfiltration and ultrafiltration membranes are both porous, it appears odd at first that different kinds of polymeric materials are utilised for both processes. A variety of microfiltration membranes are made using processes such track-etching, stretching, and sintering, which produce holes with a minimum size of between 0.05 and 0.1 μm . These methods cannot be used to create ultrafiltration membranes with holes that are smaller than a few nanometers. Phase inversion is most commonly used to prepare ultrafiltration membranes.

The polysulfones (PSf) and poly(ether sulfones) (PES) are a crucial family of polymers. The T_g values of the polysulfones (PSf: $T_g = 190^\circ\text{C}$; PES: $T_g = 230^\circ\text{C}$) show that they have extremely strong chemical and thermal stability. These polymers are frequently utilised as the building blocks for composite membranes and ultrafiltration membranes.

4.1.1.2 – Nonporous membranes

Nonporous membranes are employed in the pervaporation and separation of gases and liquids. Asymmetric or composite membranes are both employed for these procedures. The inherent features of the material govern the performance (permeability and selectivity) of this type of membrane. The kind of application will dictate the material to choose, and polymer types can range from elastomers to glassy materials [46].

Since glassy polymeric membranes provide a higher permeability and selectivity trade-off than rubbery ones, they are the industry leader for membrane gas separation. They are also relatively inexpensive and simple to reproduce. Since they age physically, the thickness of the membrane, especially when it is smaller than 1 micron, has a significant impact on their permeability over time. In case of a glassy polymer, which operates at a temperature lower with respect to its glass transition temperature, selectivity is mainly based on different diffusivity of the gas with respect to the membrane: they are characterized by high selectivity and low permeability. For instance, cellulose acetate, polysulfone (PSU), polyether sulfone (PES), polyimide (PI), polyamide (PA), polycarbonate (PC), and polyvinylidene fluoride (PVDF) are the most commonly employed polymers in membrane-based gas separation in glassy polymer materials [49].

Rubbery polymers operates at temperature higher than their glass transition temperature. The selectivity of rubbery polymers is based on solubility: they are characterized by high permeability and low selectivity [49]. The most researched polymers are poly(dimethylsiloxane), polychloroprene, polyisoprene, polyurethane (PU), butyl rubber, ethyl

propylene rubber (EPR) and poly(dimethylsiloxane). The physical interactions between gas penetrants and the polymer matrix determine the selectivity. The fact that rubbery membranes are more selective with heavier and bigger objects is one of their key properties. By increasing the molecule size, permeability capabilities improve for molecules like those of carbon dioxide. Furthermore, membranes made of rubbery polymers swell and plasticize, which are going to be analysed in the next sections.

4.1.2 – Inorganic membranes

Inorganic membranes include zeolite and carbon molecular sieve membranes. Similarly to polymeric membranes, inorganic membranes can be divided into porous and nonporous. Zeolite membranes are porous, perform well in gas separation, and are resistant to chemicals due to their hydrophobic nature. For high-temperature applications, nonporous membranes are appropriate [45]. In difficult operating circumstances, inorganic membranes have great deformation resistance. Comparatively speaking to other forms of membranes, the separation factor in inorganic membranes is likewise significantly greater. The clearly defined pore size and molecular sieving ability of such membranes are the causes of this increased separation efficiency [50]. Inorganic membranes have a limited commercial application because of their expensive cost and weak toxin tolerance [51]. As the selective layer is less than 5 micrometres thick and the rest portion provides mechanical support, one of the primary disadvantages of inorganic membranes is their thickness. Permeation does, in fact, rely on membrane thickness, with too thin membranes being too fragile to handle while bigger membranes are more resilient but have less permeability. Supported membranes are chosen since very thin self-supported ones are brittle [52].

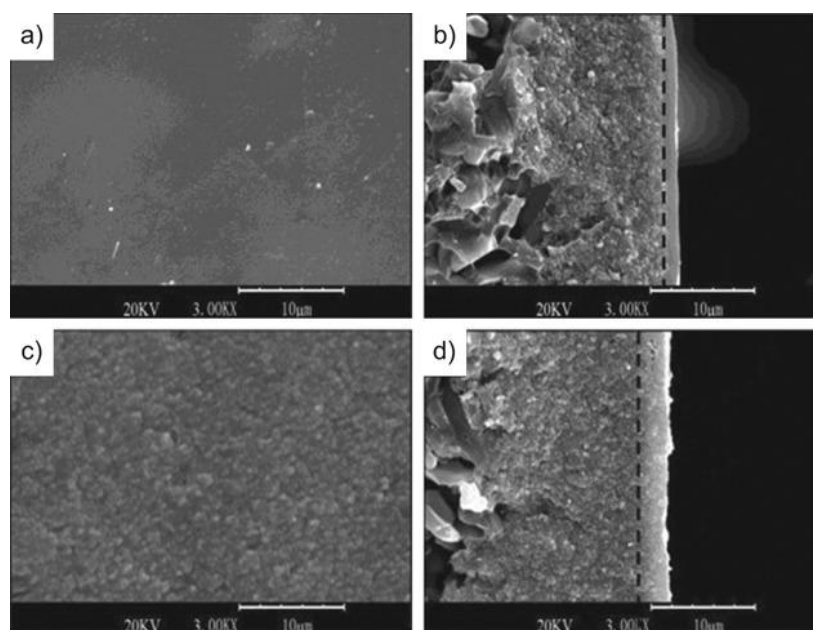


Figure 16: surface and cross-sectional SEM images of a thin zeolite T/carbon composite membrane (a, b: 0 wt.%; c, d: 1 wt.%) [53].

While dense palladium membranes are utilised for hydrogen separation, inorganic membranes with porous media, such as zeolites, glass, alumina, zirconia, and carbon membranes, reveal a transport mechanism of molecular sieving and/or adsorption diffusion [54]. Figure 16 shows a synthetic thin zeolite T/carbon composite membrane. When 2% weight of zeolite was introduced, a permselectivity of 143 was attained for the separation of CO₂/CH₄. *Figure 16* displays pictures taken using a scanning electron microscope (SEM) of synthetic zeolite membranes. The surfaces of a pure carbon membrane and this membrane with a 1% zeolite loading are seen in *Figs. 16a* and *16c*, respectively. The pure carbon membrane's smooth surface is seen in *Figure 16a*, however the addition of zeolite particles produced a rough surface, as seen in *Figure 16c*. *Figures 16b* and *16d* show the cross sections of the pure carbon membrane and the carbon/zeolite composite membrane with a 1% zeolite loading. The cross section of the zeolite composite membrane makes it simple to see whether zeolite particles are present in the membrane. In *Fig. 16d*, it is clear that the zeolite particles are distributed uniformly throughout the carbon matrix [53].

4.1.3 – Mixed matrix membranes (MMM)

Mixed matrix membranes have started to become a viable option in membrane technology in order to get around the limitations of polymeric and ceramic membranes. This solution combines the advantageous mechanical capabilities and cost-effective processability of polymers with the outstanding gas separation properties of molecular sieve materials [55]. The dispersed phase of mixed matrix membranes made of inorganic materials has a distinct structure, surface chemistry, and mechanical strength. It is anticipated that when they are added to the polymer matrix, the resulting membrane properties will be better than those of conventional polymer membranes; however, few attempts to improve the performance of gas separation membranes with MMM have been reported among the numerous studies on conventional polymers in the past three decades. This is due to the problems associated with mixed matrix membrane manufacturing, such as weak particle interaction inside the polymer matrix and uneven distribution of the dispersed phase within the continuous polymer matrix phase. Moreover, the mixed matrix characteristics can be impacted by polymer type and properties, dispersed phase load, particle size and particle pore size [56].

Polymer having a combination of glassy and rubbery qualities, such as polyether block amide (Pebax), has also been added to the MMM production process to enhance the gas separation capabilities. This polymer has rigid (glassy) polyamide segments that offer mechanical strength, and it also has flexible (polyether) segments that are crucial for CO₂ transport [57]. Free volume, polymer polarity, and shape are only a few of the elements that might have an impact on the gas transport characteristics in the polymeric phase [58]. For example, increasing a polymer's free volume will enhance its gas diffusivity because more gas molecules may diffuse through the inefficient packing of the polymer chain. Conversely, CO₂ molecules having a strong quadrupole moment can interact with polymers containing polar functional groups more effectively. Higher CO₂ solubility in the polymer results as a result [59].

In case of presence of inorganic particles, MMMs can be divided with the classification of simple inorganic membranes by the size of the pores, hence nonporous or porous particles. The porous inorganic particles often outperform the Robeson plot in terms of separation performance due to their exact pore dimensions. Theoretically, it can be supposed that the addition of porous fillers to a polymer phase will lead to the creation of an ideal MMM that has higher selectivity than pure polymer. The porous structure of the fillers makes it easier for targeted species to be transported by gas, which can also improve the permeability of desirable gas molecules like CO₂. The enhancement in MMM's permeability and selectivity, however, can only be attained if the polymer chain completely encircles the particles and there are no interfacial flaws at the polymer/filler interface [60]. Zeolites are among the porous inorganic materials that are frequently employed in the manufacture of MMMs as fillers and CO₂ adsorbents. Zeolites are desirable because they have pores that are between 0.5 and 1.2 nm in size and can separate gas molecules with almost identical kinetic diameters (kinetic diameter of CO₂ and CH₄ equal to 3.3 Å and 3.8 Å) [59].

4.2 – Transport mechanisms

4.2.1 – Transport in non porous (dense) membranes

Fundamentally, a solution-diffusion process may be used to describe how a gas, vapour, or liquid is transported over a thick, nonporous membrane [46]. It can be defined as

$$P = D \cdot S \quad (1)$$

Where P is the permeability, D is the diffusivity and S is the solubility. Solubility is a thermodynamic characteristic and offers a measure of the quantity of penetrant sorbed by the membrane under equilibrium circumstances. Given that the diffusion coefficient decreases with increasing molecule size, diffusivity is a function of the shape of the penetrant. In polymers gas diffusion is assumed constant. The Langmuir "hole-fitting" solubility and the Henry's law "dissolved" solubility make up the sorption isotherm in the dual mode sorption theory

$$C = kp + \frac{C'_H bp}{1 + bp} \quad (2)$$

where k is the Henry's law, p is the pressure C'_H is the Langmuir capacity constant and b is the Langmuir affinity constant. Permeability can be easily described by Fick's first law

$$J = -D \frac{dc}{dx} \quad (3)$$

Which states that flux J is directly proportional to the change of concentration and D is the diffusion coefficient. Henry's law, which states that there is a linear connection between the external pressure p and the concentration c inside the membrane, may be used to describe the solubility of a gas in a membrane

$$c = S \cdot p \quad (4)$$

If last two equations are put in relation and an integration across the membrane thickness is performed, flux can be described as

$$J = \frac{S D}{l} (p_1 - p_2) \quad (5)$$

Where p_1 and p_2 are the feed and permeate pressures. With the correlation between P, D and S, flux can be directly related to permeability with the following equation

$$J = \frac{P}{l} (p_1 - p_2) \quad (6)$$

This equation demonstrates that the flow of a component across a membrane is inversely related to membrane thickness and directly proportional to the pressure differential across the membrane.

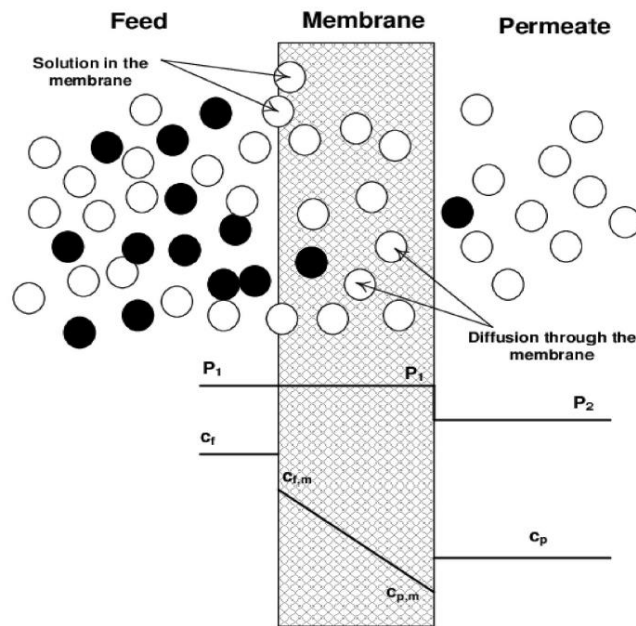


Figure 17: scheme of dense membrane separation mechanism [61].

Looking at *figure 17*, there are three streams in gas separation systems: the feed stream, that is the initial gas mixture at higher pressure, the permeate stream, which is the gas flux that passed through the membrane, and the retentate stream, that has not crossed the membrane.

In order to compare different kind of membranes, it can be useful to compare the permeance, which is defined as

$$Permeance = \frac{P_i}{L} \quad (7)$$

where P_i is the gas permeability and L is the membrane thickness. Permeability is calculated as

$$P = \frac{\dot{Q} \cdot L}{A \cdot \Delta p} \quad (8)$$

where \dot{Q} is the volumetric flowrate, A is the surface of the membrane and Δp is the pressure difference between the feed pressure and the permeate. Commonly, the permeability is measured in barrer, which is equivalent to

$$1 \text{ Barrer} = \frac{cm^3(STP)cm}{cm^2s \text{ cmHg}} \cdot 10^{10} \quad (9)$$

while permeance is calculated in GPU, which is equivalent to

$$1 \text{ GPU} = \frac{cm^3(STP)}{cm^2s \text{ cmHg}} \cdot 10^6 \quad (10)$$

As illustrated in the equation (1), permeability is directly related to diffusion and solubility factors. Solution-diffusion model can be studied from a thermodynamic point of view: similarly to the Arrhenius equation, it is possible to define diffusivity as

$$D_i = D_{i0} \exp \left[\frac{-E_d}{RT} \right] \quad (11)$$

where D_i is the diffusion coefficient, D_{i0} is pre-exponential factor, E_d is the activation energy diffusion, R is the universal gas constant and T is the temperature. In a similar way solubility can be expressed using the Van 't Hoff relationship

$$S_i = S_{i0} \exp \left[\frac{-\Delta H_S}{RT} \right] \quad (12)$$

where S_{i0} is the pre-exponential factor and ΔH_S is the enthalpy of solution of the gas [47]. If both (8) and (9) are related taking into account (1), permeability can be defined as

$$P_i = P_{i0} \exp \left[\frac{-E_P}{RT} \right] \quad (13)$$

where P_{i0} is the pre-exponential factor and $-E_P$ is the activation energy of permeation, defined as

$$E_P = E_D + \Delta H_S \quad (14)$$

4.2.2 – Transport in porous membrane

The gas molecules will typically diffuse from the side with the high pressure to the side with the low pressure when an asymmetric membrane or composite membrane is employed for gas separation. An example of porous transport system is the Knudsen flow. The mean free route of the diffusing molecules becomes comparable to or bigger than the pore size of the membrane if the pores are smaller and/or when the gas pressure is dropped. Collisions with the pore wall happen more frequently than collisions between gas molecule. This is the gas transport in Knudsen flow.

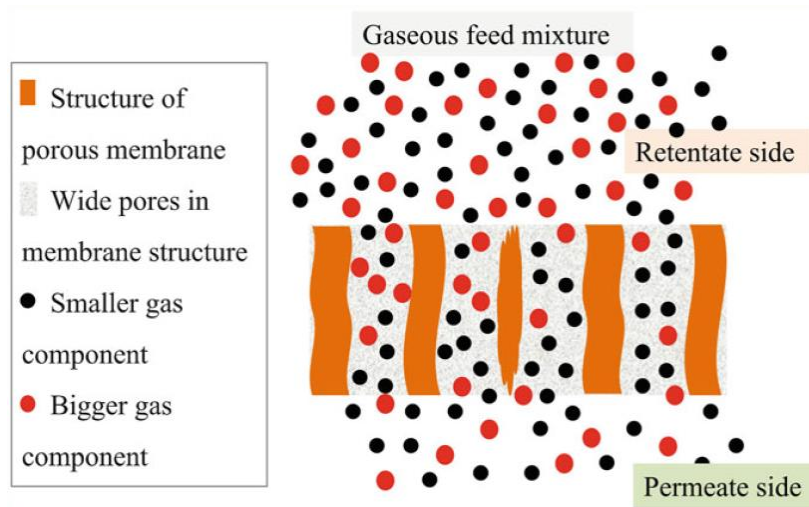


Figure 18: Knudsen diffusion mechanism [62].

The average distance a molecule travels between collisions might be referred to as the mean free path (λ). In a liquid, the molecules are relatively near to one another, and the mean free path is only a few Angstroms. Knudsen diffusion is thus not necessary in liquids. The mean free route of gas molecules, however, will be influenced by temperature and pressure. The mean free route in this situation is denoted by

$$\lambda = \frac{k T}{\pi d_{gas}^2 P \sqrt{2}} \quad (15)$$

At low pressure, flux can be described as

$$J = \frac{\pi n r^2 D_k \Delta p}{R T \tau l} \quad (16)$$

Where D_k is the Knudsen diffusion coefficient, which is equal to $D_k = 0.66 r \sqrt{\frac{8 R T}{\pi M_W}}$. T and M_W are the temperature and molecular weight and r is the pore radius.

4.3 – Technical limitations

4.3.1 – Robeson upper bound related to dense polymeric membranes

For a dense polymeric membrane, selectivity of the component i with respect to component j is given by their permeability ratio as

$$\alpha_{\frac{i}{j}} = \frac{P_i}{P_j} = \left(\frac{D_i}{D_j} \right) \cdot \left(\frac{S_i}{S_j} \right) \quad (17)$$

where D_i/D_j represents the diffusivity selectivity and S_i/S_j represents the solubility selectivity.

In order to reduce the energy costs associated with gas compression and to decrease the membrane's active surface area, membranes with very high permeance (i.e. flux) are desirable for gas separations on such a large scale. This will optimise the membrane system's overall size and manufacturing cost. However, established ultrapermeable polymers, such as polyacetylene poly(trimethylsilylpropyne) (PTMSP) [63] and recently reported examples are insufficiently selective for use in gas separations because polymer membrane materials suffer from the well-established trade-off between gas permeability (P_x) and selectivity for one gas over another (P_x/P_y) by Robeson [64]. Robeson established upper bounds in plots of $\log(P_x/P_y)$ versus $\log P_x$ for various gas mixtures (O_2/N_2 , H_2/N_2 , He/N_2 , H_2/CH_4 , He/CH_4 , CO_2/CH_4 , and He/H_2) based on the gas permeability of the best-performing polymers at the time in 1991, thereby quantifying the general trade-off between polymer permeability and selectivity for the first time. Its potential for gas separations may then be calculated based on where its gas permeability measurements lie in relation to the upper boundaries of Robeson plots [65]. Using preliminary results for two spirobisindane-based Polymers of Intrinsic Microporosity (PIM-1 and PIM-7), whose stiff and twisted macromolecular architectures produced very high permeability with moderate selectivity, Robeson revised all of the upper limits in 2008 [66].

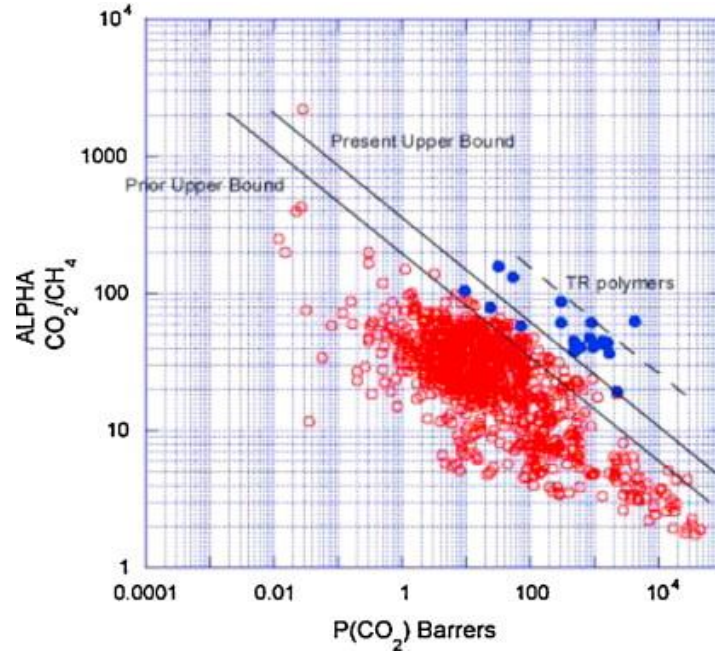


Figure 19: trade-off behaviour and limit of CO₂/CH₄ gas permeation membranes [66].

The upper bound relationship is expressed by

$$P_i = k \alpha_{ij}^n \quad (18)$$

where P_i is the permeability of the more permeable gas between the two analyzed, α is the selectivity and n is the slope of the curve; for the 2008 upper bound, $k=5369140$ and $n=-2.64$ [66].

4.3.2 – Swelling

Swelling is a significant issue with polymeric membranes for the separation of CO₂/CH₄. It is one of the crucial elements that must be taken into account when choosing the type of membrane material. When the polymer dissolves in the specified solvent or as a result of feed moisture, swelling happens. Since it modifies the polymer's physical and chemical structure, membrane swelling is essential for the passage of molecules through a membrane [67]. Three phases make up the swelling process. The solvent or swellant is absorbed into the polymer surface in the first stage. The second stage is when the solution enters the polymer to occupy free volume. The third phase involves the solvent getting within the polymer chains. More liquid can pass through because of the increase in free volume brought on by the swelling of dense polymers. As a result, it affects the membrane's permeability and selectivity. Swelling impacts membrane transport through two different processes. Due to the increase in permeability brought on by swelling, the free volume of the membrane expands. As a result of the membrane swelling, the membrane's selectivity declines [68].

Membrane swelling typically takes place in offshore feed situations with high feed humidity. Water works as a swelling agent under these circumstances, causing membrane swelling at greater pressures. Water vapours enter the polymer matrix at greater pressures because of the humidity in the feed, changing the molecular structure of the polymer. As a result, the disturbance in polymer structure has an impact on separation performance. Hence, it is essential to manage the behaviour of membrane swelling, particularly in offshore feed circumstances and at greater pressures [69].

One of the easiest and most practical ways to deal with membrane swelling is cross-linking. Chemical cross-linking, thermal processing, cross-linking using UV radiation, and ion beam cross-linking are some of the possible techniques for polymer modification by cross-linking [70]. Cross-linking improves the chemical and thermal durability of membranes while reducing their tendency to swell. Because of the decreased chain mobility, the glass transition temperature rises as a result. By fostering the molecular connections between the polymer chains, a decrease in chain mobility minimises swelling. Chemical cross-linking typically takes place at ambient temperature [71].

4.3.3 – Plasticization

The other main issues with membrane-based CO₂/CH₄ separation is CO₂-induced plasticization. Different penetrants dissolve into the polymer matrix during plasticization, destroying the structure of the polymer in the process. It is pressure-dependent and mainly happens at high pressures. The main contributors to plasticization are heavy hydrocarbons and condensable gases like CO₂. In CO₂-induced plasticization, the membrane's selectivity is significantly reduced as CO₂ permeability rises. The polymer structure is altered by the swelling of the interchain spaces caused by dissolved CO₂ [72]. Penetrants have a direct impact on the separation process by diffusing widely throughout the polymer matrix. In addition to suppressing the polymer's glass transition temperature, plasticization also somewhat depends on the thickness of the membrane. It has been demonstrated that thicker membranes are more resistant to plasticization than thin sheets. Thus, it is essential to find a solution to the plasticization issue, particularly under harsh feed circumstances with high CO₂ and significant hydrocarbon content [73].

The most appealing method to prevent CO₂-induced plasticization of membranes is cross-linking. It raises the pressure at which plasticization takes place and improves the membrane's separation capabilities for the separation of natural gas. It increases membrane stability at increased CO₂ partial pressure. Membranes that have been cross-linked can be employed in harsh feed circumstances [74]. The most straightforward, cost-efficient, and efficient method of bringing about alterations on the polymer surface is thought to be chemical cross-linking. This approach is popular since it typically involves room temperature cross-linking of various polymer components [75]. Thermal treatment, also known as thermal cross-linking, is a process whereby chemical cross-linking is followed by heating at different temperature ranges [76].

A novel method for creating more effective polymeric membranes for gas separation is polymer sulfonation. Sulfonated monomers are employed in this method to create a polymer. The membrane is then created using synthetic sulfonated polymer. The degradation of the polymer's mechanical and thermal stabilities is the only drawback of this technique. Polymeric materials that can work at high temperatures and under demanding feed conditions are now required since polymeric membranes are widely used in gas separation. To thermally rearrange the structure of polymeric materials, they are heated to certain temperatures. During thermal rearrangement, the polymer's thermal stability rises. The creation of hollow-fiber membranes was the first use of this method [76].

Another method for resolving the plasticization issue in polymeric membranes is polymer mixing. Polymer blending involves combining two or more polymers in various ratios to create a mixture. After mixing, the polymers' mechanical and thermal characteristics improve. To a certain extent, polymer mixing can prevent plasticization. The fabrication of polymeric membranes with high performance has been documented in the literature using a variety of polymer blends. Polyetherimide (PEI)/polyetheramide (PEA), polybenzimidazole (PBI)/polyetherimide (PEI), polyethylene glycol blends, and polyimide blends are a few of the polymer blends that have been documented in the literature [77]. The miscibility of polymer mixtures is one of the issues with polymer mixing. Various polymer classes are not miscible with one another, which causes the membrane to develop spongy shapes [78].

An additional technique to improve the stability and resistance of membranes to plasticization is polymer grafting. In polymer grafting, an aromatic chain or other short, stiff chain of a separate polymer is introduced into the polymer matrix. At greater pressures, this method can also partially prevent plasticization [79].

5 – Experimental setup

In this chapter a review of the tested membrane and experimental bench will be discussed. For the membrane section, a brief description in composition, preparation techniques and expected performances will be given. Then, a description of membrane testing machine is carried out, followed by the two ways that were adopted to evaluate membrane permeability. For all the tests only pure gas permeability were tested, hence no mixture composition will be discussed.

5.1 - Tested membrane

In this section a description of tested membrane structure and production methods will be explained. For PES-WC and PEEK-WC membrane preparation similar procedures have been applied.

5.1.1 – Matrimid

Matrimid 5218 membrane is obtained by the polycondensation of BTDA (3,3',4,4'-benzophenone tetracarboxylic dianhydride and diaminophenylindane) and a mixture of two cycloaliphatic monomers, such as 5,6-amino-1- (40-aminophenyl) and 1,3,3-trimethylindane. The structure is represented in *figure 20*. The solvent was then allowed to evaporate overnight in a clean hood before the resulting film was placed in a vacuum oven at 200 °C [80]. This polymer has an approximate T_g of 320 °C and average molecular weight of 80000 g/mol [81].

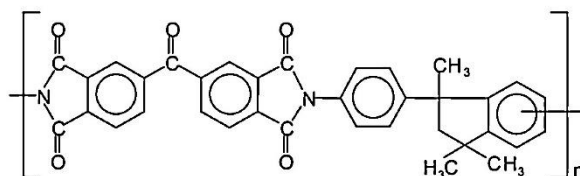


Figure 20: Matrimid chemical structure [82].

Matrimid, and polyimides in general, are glassy polymers that are distinguished by an excess of free volumes that contribute to the gas transport qualities, bestowing suitable selectivity and permeability values. As a result, a variety of uses for this polymer are possible, notably as a continuous phase for the separation of organic (such as CH₄, C₂H₄, C₂H₆, C₃H₆, C₃H₈, and C₄H₁₀ gases) and inorganic gases (i.e., CO₂, H₂, CO, N₂, SF₆, O₂, and Ar) [83].

T _g [°C]	Thickness [μm]	Permeability CO ₂ @25°C [Barrer]	Permeability CH ₄ @25°C [Barrer]	Selectivity	FV	Density [g/cm ³]
310	25	8.4	0.16	52.5	0.17	1.2

Table 4: Matrimid reference characteristics [84].

Matrimid permeability to CO₂ and selectivity between CO₂ and CH₄ are illustrated in *table 5*. Because of its well known and stable values, this membrane was used as validation for the test

bench, hence recorded values were compared to the known ones. Main differences between reference data and tested membrane are membrane thickness ($t_{\text{ref}} = 25\mu\text{m}$, $t_{\text{test}} = 80\mu\text{m}$) and working temperature ($T_{\text{ref}} = 25\text{ }^\circ\text{C}$, $T_{\text{test}} = 20\text{ }^\circ\text{C}$).



Figure 21: Matrimid membrane tested in our bench.

5.1.2 - PES-WC

Polyethersulfone (PES) is one of the most significant polymers in the separation sciences. For this work, a blend of PES with WC was tested. It was provided by chemistry department of UNITO (Turin).

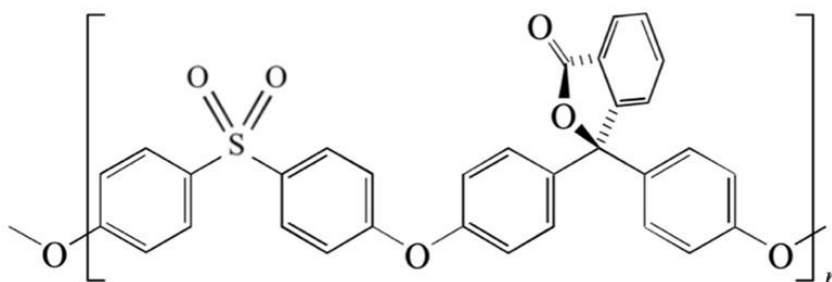


Figure 22: PES-WC chemical structure.

Polymeric solution of PES-WC membrane preparation has been characterized by solubilisation of 2.5147g of PES-WC in 15 mL of dimethylformamide (DMF), reaching a mass ratio of 15%. The obtained solution was then left stirring for a minimum of 24 hours. After that, membrane has been subjected to a thermal treatment. It was laid out on a glass plate using a filmograph and left for 24 hours at $40\text{ }^\circ\text{C}$, then it was left in a vacuum heater at $120\text{ }^\circ\text{C}$ and 27 mbar for 6 hours. Finally, membrane was detached from the glass plate.



Figure 23: PES-WC membrane made by chemical department of UNITO and tested in our bench.

Another PES-WC membrane was mixed with β -CDNS cyclodextrin nanosponge with 1% of mass ratio. In this case procedure has been the same as referred before.

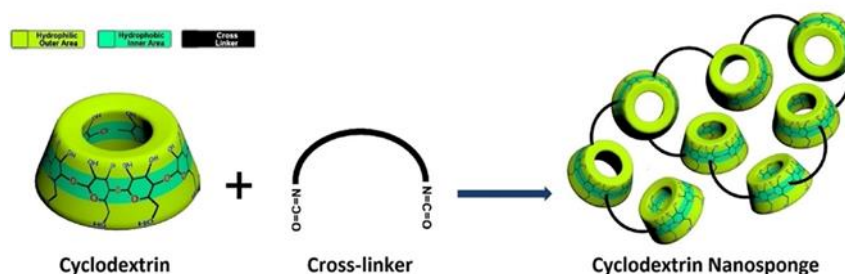


Figure 24: schematic representation of cyclodextrin nanosponge [85].

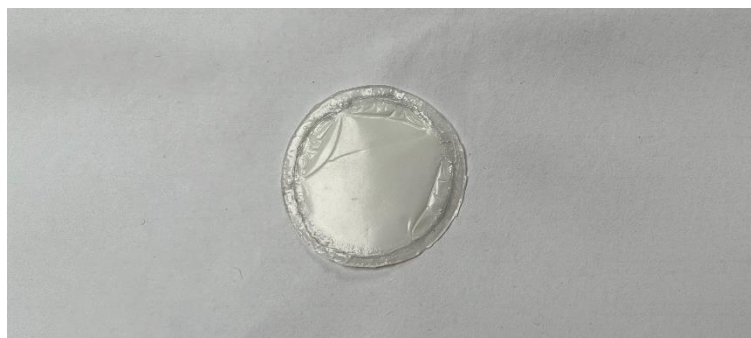


Figure 25: PES-WC with cyclodextrin nanosponge made by chemical department of UNITO and tested in our bench.

5.1.3 - PEEK-WC

PEEK-WC (or PEEKWC, PEK-C) has been utilised extensively in membrane synthesis and characterization [86]. Also PEEK-WC membrane was provided by chemistry department of UNITO (Turin).

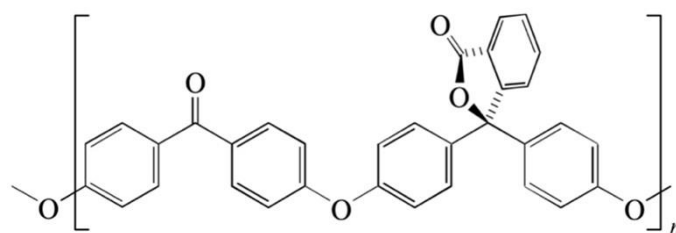


Figure 26: PEEK-WC chemical structure.

Similarly to PES-WC membrane preparation, PEEK-WC has been characterized by solubilisation of 2.5147g of PEEK-WC in 15 mL of dimethylformamide (DMF), reaching a mass ratio of 15%. The obtained solution was then left stirring for a minimum of 24 hours. After that, membrane has been subjected to a thermal treatment. It was laid out on a glass plate using a filmograph and left for 24 hours at 40 °C, then it was left in a vacuum heater at 120 °C and 27 mbar for 6 hours. Finally, membrane was detached from the glass plate.



Figure 27: PEEK-WC made by chemical department of UNITO and tested in our bench.

5.2 – Experimental CO₂ capture system test rig

The experimental test rig is located in the CO₂ circle lab (CCL) in Environment Park (Turin, Italy). Environment Park is a Technology Park that has been active for over 20 years in environmental innovation and sustainability. It is a private company with public shareholders. In the CO₂ circle lab (CCL) there are many test benches related to CO₂ capture and utilization: in this work tests were performed with the “CO₂ capture system test” bench.

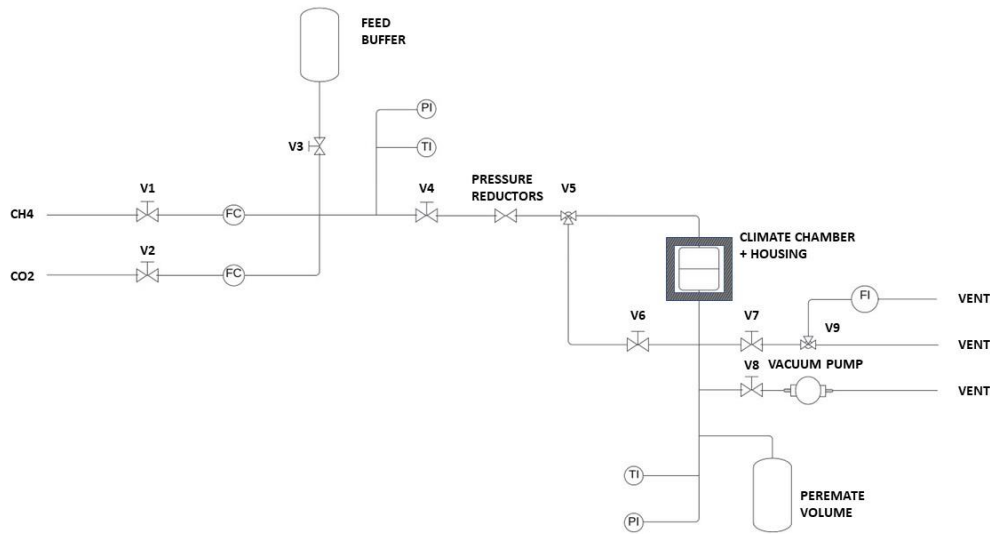


Figure 28: scheme of the “CO₂ capture system test” bench.

“CO₂ capture system test” bench is supplied with different pressurized gases: these are N₂, H₂, CO₂, CO, CH₄ and O₂. For the tested membranes only CO₂ and CH₄ have been employed, hence in the scheme in *figure 28* they are the only gases represented. Line pressure ranged between 20 bar and 30 bar. Switch valves V1 and V2 let CH₄ and CO₂ go through the test bench, while two Bronkhorst Thermal Mass Flow Meters and Controllers (FC) are able to adjust the gas flux between 0 and 100 ml/min. V3 is a switch valve: it let the gas go in a 1L buffer, which is a feed reservoir. V4 let the gas go through a series of two pressure reducers: these are able to stabilize the outlet pressure, albeit buffer pressure change during a test.



Figure 29: two pressure reducers in series able to stabilize feed pressure during tests.

V5 is a three-way valve that can make the gas go towards the feed side of the membrane, the permeate side or both. The climate chamber is a cell made by FDM in which the housing is located: it can set the temperature in a range between -20°C and 80 °C with a precision of ±0.1°C. The housing is a device in which the tested membranes are placed: it is divided into

feed side and permeate side. V6 is another valve able to isolate permeate side from feed side. There is a pressure indicator in the permeate side able to acquire pressure data: its range is between 0 bar and 10 bar and its precision is ± 0.005 bar. The permeate buffer volume is 20.76 cm^3 , with $\pm 1.72 \text{ cm}^3$ uncertainty: Volume was calculated by monitoring pressure in a gas expansion from a known volume to the permeate volume (put under vacuum condition before expansion): as carbon dioxide was employed in gas expansion, it was taken into account compressibility factors of non-ideal gases by applying Peng-Robinson equation. V7 connects the permeate side with the vent and the volumetric flowrate instrument (range between 5 ml/min and 550 ml/min with a precision of ± 0.01 ml/min): the flow can go directly to the VENT (ventilation at low depression, 0.99 bar) or through the flowrate indicator (which discharges to the VENT) based on V9 position. In order to evacuate any gases in the circuit there is a vacuum pump system able to decrease pressure down to $1 \cdot 10^{-4}$ bar.



Figure 30: housing in a climate chamber, with feed in higher side and permeate in the lower side.

There are two ways to acquire data: the closed volume configuration and the open system configuration. Both are described in the next sections. It is important to underline that leakages in the permeate side are neglected: with initial and final experiment pressure in the permeate side in the range between 1.00 bar and 1.30 bar, leakage rate has always shown at least one order of magnitude lower than permeate gas flowrate.

5.2.1 - Closed volume test

The closed volume configuration measures the permeate flux by monitoring the pressure increase in a closed volume. The pressure is acquired with a pressure transducer. The constant volume method has been employed when volumetric flowrate through the membrane was lower than 5 ml/min.

Before a new membrane is tested or new gas is sent to the feed side, vacuum conditions in the circuit is set in order to remove any volatile impurities or air gases: this procedure usually lasted 12 hours (the night before the first acquisition). All valves are open, except for V1, V2 and V7. Pressure in the system is in the order of 10^{-3} bar. After that, vacuum pump is disconnected, V8 and V4 are closed. At this point, V1 or V2 are opened, based on the desired gas. Then the flow rate is set with the FC. Pressure in the feed reservoir increase: usually FC is closed when pressure in the feed reservoir is between 10 and 15 bar. After that, pressure reducers are closed and then V4 is opened. Now pressure reducers are set to have the output pressure equal to the desired feed membrane pressure: for this work, feed pressure range was between 2 and 10 bar. In order to set the feed pressure, during regulation V5 is set to send the gas both in the feed and permeate side, V6 is opened: pressure is read in the permeate pressure indicator. When permeate PI shows the desired feed pressure, gas in the permeate side has to be evacuated through the vent: V6 is closed, V7 is opened and V9 is set to send the gas directly to VENT. When PI in the permeate side shows 0.99 bar, V7 is closed and V5 is set to send gas to the feed side only. Now the acquisition can start by saving permeate PI values in time. Acquisition should last until the change of pressure in time can be supposed linear: for this work acquisition was completed when

$$P_{perm} = 1.00 \text{ bar} + (0.03 \cdot \Delta p) \text{ bar} \quad (19)$$

where P_{perm} is the pressure showed by permeate PI and Δp is the pressure difference between feed side and permeate side (this value ranged between 1 bar and 9 bar). 0.03 coefficient is a compromise between acquiring enough data and having the supposed linear trend.

When acquisition is completed, permeate side should be evacuated in order to start another acquisition. First of all, acquisition is stopped, then V7 and V9 are opened and permeate gas is sent directly to VENT. As explained in the previous section, when permeate PI shows 0.99 bar, V7 is closed. New acquisition can start by saving permeate PI values in time in another data file.

When another feed pressure need to be set, V5 is set to send the gas both in the feed and permeate side and V6 is opened. When permeate PI shows the desired feed pressure, gas in the permeate side has to be evacuated through the VENT: V6 is closed, V7 is opened and V9 is set to send the gas directly to VENT. When PI in the permeate side shows 0.99 bar, V7 is closed, V5 is set to send gas to the feed side only and a new acquisition can start.

5.2.2 - Open system test

The open volume configuration measures the permeate flux by directly measuring volumetric flowrate through the tested membrane. Volumetric flowrate is acquired with a MesaLabs Bios DryCal Definer 220. The open system method has been employed when volumetric flowrate through the membrane was higher than 5 ml/min.

Before a new membrane is tested or new gas is sent to the feed side, vacuum conditions in the circuit is set in order to remove any volatile impurities or air gases: this procedure usually lasted 12 hours (the night before the first acquisition). All valves are open, except for V1, V2 and V7. When pressure in the system is in the order of 10^{-3} bar, vacuum pump is disconnected, V8 and V4 are closed. At this point, V1 or V2 are opened, based on the desired gas. Then the flow rate is set with the FC. Pressure in the feed reservoir increase: usually FC is closed when pressure in the feed reservoir is between 10 and 15 bar. After that, pressure reductors are closed and then V4 is opened. Now pressure reductors are set to have the output pressure equal to the desired feed membrane pressure: for this work, feed pressure range was between 2 and 10 bar. In order to set the feed pressure, during regulation V5 is set to send the gas both in the feed and permeate side, V6 is opened: pressure is read in the permeate pressure indicator. When permeate PI shows the desired feed pressure, gas in the permeate side has to be evacuated through the vent: V6 is closed, V7 is opened and V9 is set to send the gas directly to VENT. Differently to closed volume case, permeated gas is always discharged in VENT through V7. After 30 minutes of working conditions, volumetric flowrate is acquired each 15 minutes for 4 times. The acquisition procedure is defined by some steps: volumetric flow indicator is switched on and set to begin the flow calculation, V9 is set to send gas only in the flow indicator, volumetric flow result is manually copied in a data file, V9 is set to send gas directly to VENT and volumetric flow indicator is switched off.

When another feed pressure need to be set, V7 is closed, V5 is set to send gas both in the feed and permeate side and V6 is opened. When permeate PI shows the desired feed pressure, gas in the permeate side has to be evacuated through the VENT: V6 is closed, V7 is opened and V9 is set to send the gas directly to VENT. As before, after 30 minutes of working conditions, volumetric flowrate is acquired each 15 minutes for 4 times.

6 - Data filtering and evaluation

In this chapter data analysis and methods for permeability evaluation are carried out. First sections describe the digital data transcription, noise signal magnitude and precision evaluation. Then another part shows how those issues were managed. Finally, permeability evaluation for both closed and open volume are exposed.

6.1 - Raw data analysis in closed volume case

Main issue about data evaluation were about the big raw data files and noise/precision issue. In open volume tests data were not acquired with a digital acquisition system, hence next sections are strictly related to closed volume case.

6.1.1 - Acquisition transcription

In closed volume tests, pressure was recorded with an Omega pressure transducer: its range is between 0 bar and 10 bar and its precision is ± 0.005 bar. In the saved file other data were acquired, such as time, different test bench temperature and pressures. For this work, only time and permeate pressure were considered, since temperature was supposed equal to the one set by the climate chamber (20°C) and feed pressure was set before any acquisition.

For the acquisition a software called “Software CO2 CAP TEST001” was used. The digital acquisition system has a sampling frequency of 300 Hz. In each line of the saved data file were acquired 11 different columns, in which the first was the time, then 5 columns about temperature followed by 5 columns about pressure were recorded. Main issue about data storage procedure concerns the repetitive saving of the same line for more than 500 times, except for the acquisition time. Each acquisition stored 50MB every 30 minutes and some of them lasted more than 40 hours. This made data file really big and difficult to quickly analyse for the permeability evaluation. An example of stored data is given in *table 5*.

line	Time [s]	T1 [°C]	T2 [°C]	T3 [°C]	T4 [°C]	T5 [°C]	P0 [bar]	P1 [bar]	P3 [bar]	MKS [mbar]	P4 [bar]
1	23.3338	16.8084	15.8783	19.1337	20.1066	20.5325	1.5675	0.0097	1.0054	0.1057	0.9217
2	23.3378	16.8084	15.8783	19.1337	20.1066	20.5325	1.5675	0.0097	1.0054	0.1057	0.9217
3	23.3418	16.8084	15.8783	19.1337	20.1066	20.5325	1.5675	0.0097	1.0054	0.1057	0.9217
.
.
.
263	24.1434	16.8084	15.8783	19.1337	20.1066	20.5325	1.5675	0.0097	1.0054	0.1057	0.9217
264	24.1474	16.8084	15.8783	19.1337	20.1066	20.5325	1.5675	0.0097	1.0054	0.1057	0.9217
265	24.1504	16.8084	15.8783	19.1337	20.1066	20.5325	1.5675	0.0097	1.0054	0.1057	0.9217
266	24.1534	16.8037	15.8726	19.1293	20.1029	20.5302	1.5678	0.0096	1.009	0.1057	0.9225
267	24.1564	16.8037	15.8726	19.1293	20.1029	20.5302	1.5678	0.0096	1.009	0.1057	0.9225
268	24.1603	16.8037	15.8726	19.1293	20.1029	20.5302	1.5678	0.0096	1.009	0.1057	0.9225
.
.
.
823	25.9303	16.8037	15.8726	19.1293	20.1029	20.5302	1.5678	0.0096	1.009	0.1057	0.9225
824	25.9333	16.8037	15.8726	19.1293	20.1029	20.5302	1.5678	0.0096	1.009	0.1057	0.9225
825	25.9363	16.8037	15.8726	19.1293	20.1029	20.5302	1.5678	0.0096	1.009	0.1057	0.9225
826	25.9403	16.8013	15.8702	19.1252	20.1031	20.5341	1.5678	0.0096	1.012	0.1057	0.9233
827	25.9433	16.8013	15.8702	19.1252	20.1031	20.5341	1.5678	0.0096	1.012	0.1057	0.9233
828	25.9463	16.8013	15.8702	19.1252	20.1031	20.5341	1.5678	0.0096	1.012	0.1057	0.9233

Table 5: example of a raw data acquisition. Data in lines were repeated for more or less 500 times, except for the time column. The change in values is highlighted with a double line.

For what concerns open volume tests, a reading of the flowmeter instrument has been done. The reading is a mean value between 10 successive acquisitions (interval of 1s to 15s). Then value is manually saved in a data file with the acquisition time.

6.1.2 – Noise and precision evaluation

Pressure change evaluation has occurred only in closed and fixed volume tests. Acquired pressure is referred to permeate side pressure of the membrane. That side is always at lower pressure than the feed side (in our tests Δp is in the range between 1 bar and 9 bar), hence theoretical permeate pressure derivative should be always positive.

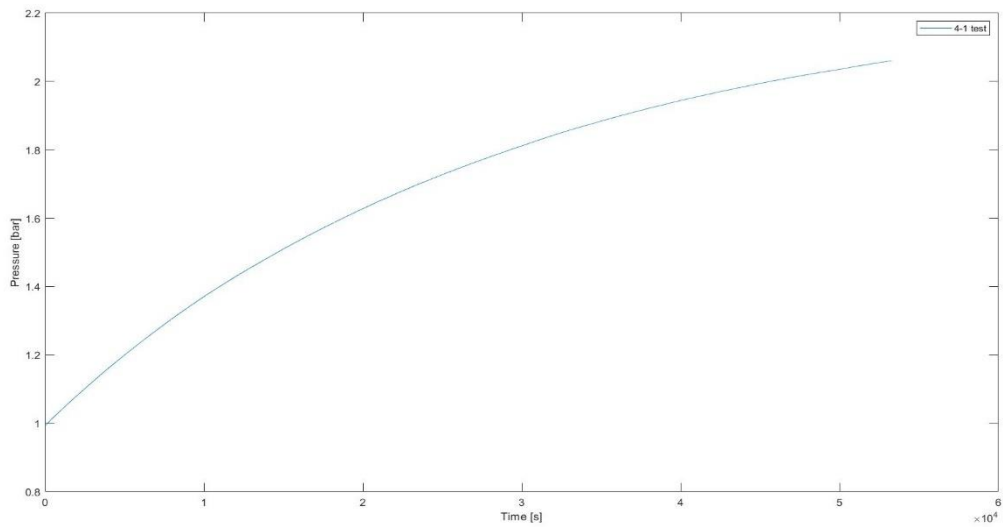


Figure 31: evolution of permeate pressure of a PES-WC (15% polymer blend) with a cyclodextrin nanosponge β CD:NSI 1:4, feed pressure equal to 4 bar and permeate pressure at the beginning of the test equal to 0.99 bar.

In figure 31 a plot of permeate pressure evolution in time is represented. In a long term experiment a decrease of curve slope in time is expected due to the decrease in pressure difference between feed side and permeate side. In order to correctly evaluate permeability, only the first part of the experiment should be considered as its trend can be supposed linear.

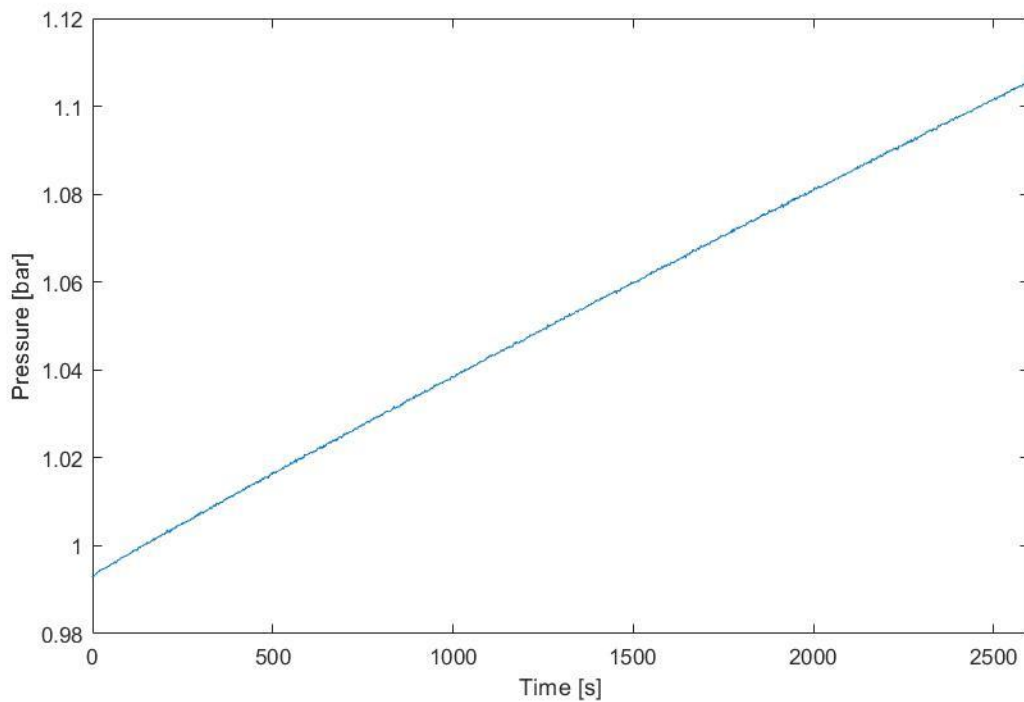


Figure 32: detail in pressure evolution of the figure 31 test.

In *figure 32* a zoom of the first 40 minutes acquisition of the plot in *figure 31* is showed. As it can be seen, the trend can be approximated to a linear one. If a more detailed look into the previous graph is done, pressure acquisition shows an irregular trend in a little time interval, as it can be seen in the *figure 33*.

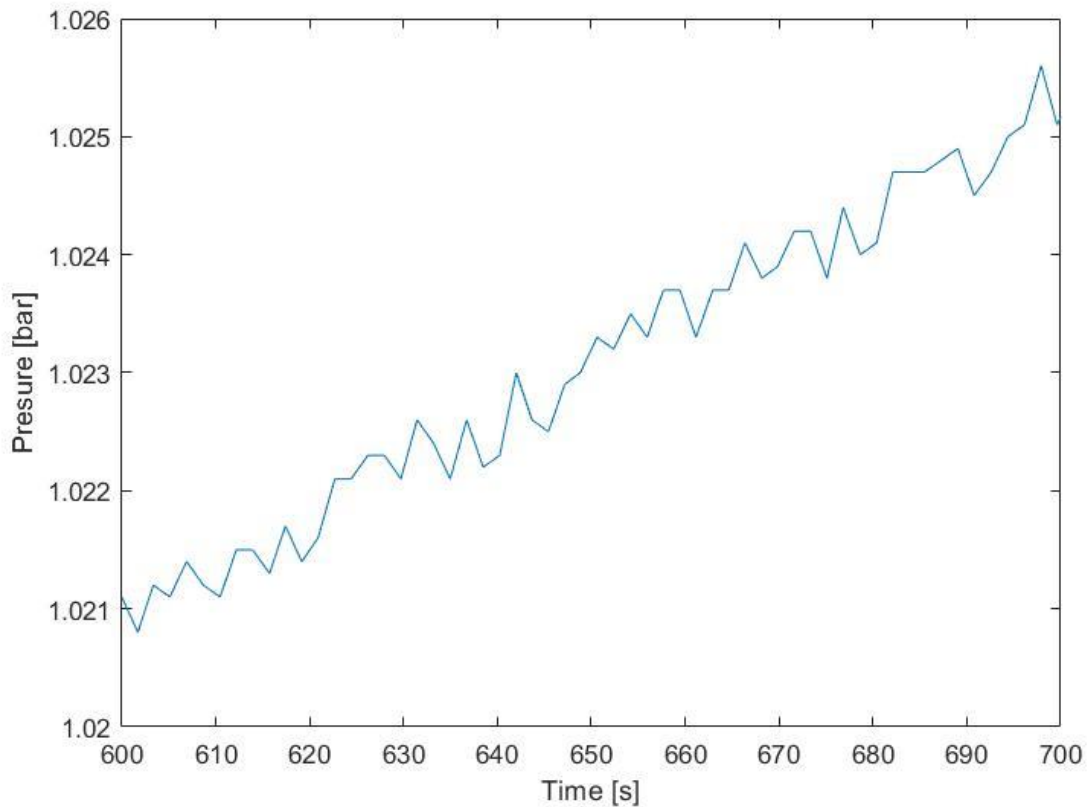


Figure 33: actual pressure acquisition trend in a shorter time interval.

Permeate pressure derivative is strictly related to membrane permeability. Any negative pressure derivative have no meaning, hence, by looking at *figure 33*, before calculating permeability pressure values should be manipulated in order to evaluate only positive pressure derivative.

6.2 - Data filtering

As explained in section 6.1.1, acquisition of experimental values implied a large amount of memory storage and acquisition of unhelpful data. Any software that directly interacted with those raw data files dealt with long operative time.

In order to overcome that issue, a decimation technique has been applied to the raw data file in order to lighten dimensions: this solution also decreases time needed from software calculator to interact with.

The main decimation steps are the following:

1. Open raw data file
2. Create a new file where only useful data are stored (decimated file)
3. Copy the first time and pressure values in the new decimated file
4. Copy time and pressure values from the raw data file when differ from the previous saved values
5. Close the new decimated file and the raw data file

In this way new decimated file dimension is 500 times lower than the raw data one.

line	Time [s]	Pperm [bar]
1	0	1.0054
2	0.8206	1.009
3	2.6075	1.012
4	4.2726	1.0154
5	5.9725	1.0189

Table 6: first lines of a new decimated file.

An example of difference between two files is given in *figure 34*.

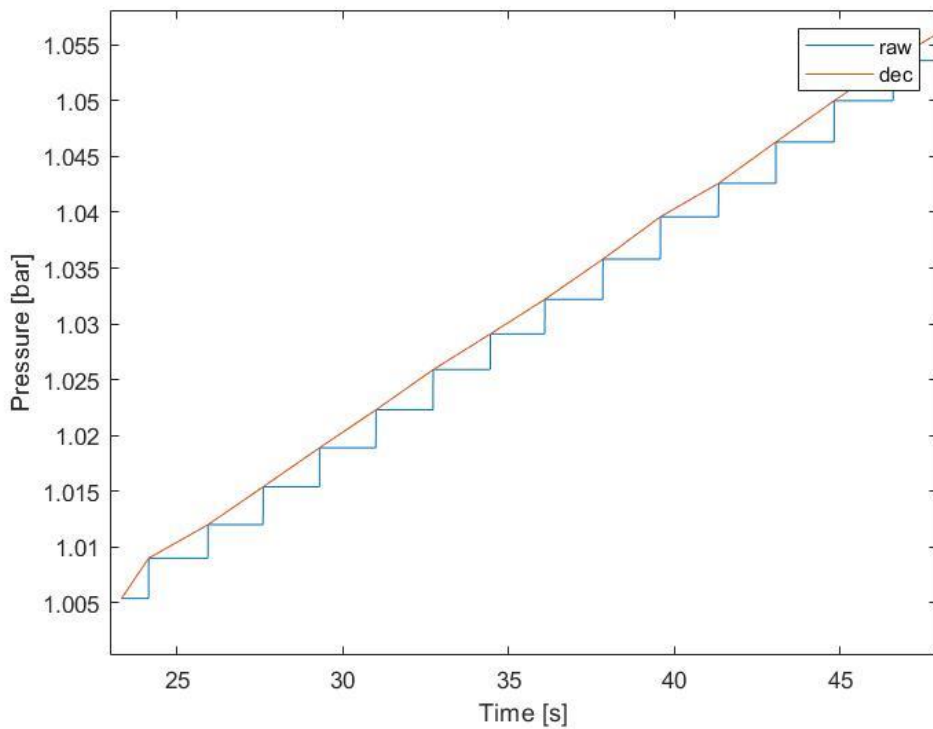


Figure 34: comparison between raw data file plot (blue line) and decimated data file plot (orange line). In each horizontal line of the raw data plot there are 500 identical values, giving the a “ladder” shape, while decimated file were characterized by the first value of each horizontal line.

6.3 - Permeability calculation in closed volume

For permeability calculation in closed volume tests was applied the following formula

$$P_i = \frac{V_d l}{\Delta p A R T} \left(\frac{dp}{dt} \right) \quad (20)$$

Where P_i is the permeability of gas i in Barrer, V_d is the permeate volume in cm^3 equal to 20.76 cm^3 , l is the membrane thickness in cm, Δp is the pressure difference between feed side and permeate side of the membrane in cmHg, A is the surface of the membrane equal to 5.91 cm^2 , R is the gas constant equal to 0.2782 $\left(\frac{\text{cm}^3 \text{cmHg}}{\text{K cm}^3_{\text{STP}}} \right)$, T is the working temperature in Kelvin (all the experiments were performed at 293.15 K) and $\left(\frac{dp}{dt} \right)$ is the derivative of permeate pressure in time in $\left(\frac{\text{cmHg}}{\text{s}} \right)$. Each membrane was tested first with CH_4 then with CO_2 . Feed pressure is increased from 2 bar to 10 bar with steps of 1 bar or 2 bar.

As explained in section 6.1.2, acquired pressure should be manipulated in order to evaluate only positive pressure derivative. The solution adopted for this work is the following:

1. Calculation of x mean values of pressure and relative time
2. Calculation of different specific permeability (using equation (20)) between different mean pressure values (and relative time)
3. Calculation of final permeability as mean between the different specific permeability calculated before.

Permeability calculation should be considered in the range where the curve slope is linear. As supposed in section 5.2.1, the equation (19) is the last useful pressure value to be evaluated. For what concern the first useful value, it was supposed a transition time in order to reach stable conditions equal to

$$t_{first} = t_{last} * 0.25 \quad (21)$$

Where t_{first} is the time of the first useful value, t_{last} is the time of the last useful value and 0.25 is an imposed coefficient. After t_{first} is calculated, the first useful pressure is the pressure value at time nearest to t_{first} .

6.4 – Permeability calculation in open volume

In open volume tests permeate pressure is kept constant at 1 bar. Permeability is calculated with the following equation

$$P_i = \frac{\dot{Q} l}{A \Delta p} \quad (22)$$

Where P_i is the permeability of the i gas in Barrer, \dot{Q} is the volumetric flowrate in $\frac{cm^3_{stp}}{s}$, l is the membrane thickness in cm, Δp is the pressure difference between feed side and permeate side of the membrane in cmHg and A is the surface of the membrane equal to 5.91 cm^2 . As explained in 6.1.1, a reading of the flowmeter instrument has been done. The reading is a mean value between 10 successive acquisitions (interval of 1s to 15s). Value is manually saved in a data file with the acquisition time. The first value is acquired after 30 minutes in order to avoid any transitory phase. Then acquisition is performed each 15 minutes for 4 times. While permeate side is kept at 1 bar, feed pressure is increased from 2 bar to a maximum of 10 bar with steps of 1 bar. In some cases volumetric flow could have overcome the Full-Scale output (FSO) of the instrument, with the risk of irreversible damage: in order to preserve the instrument, if at a certain Δp volumetric flowrate was between 85% and 90% of FSO, no more data with higher feed pressure were acquired. Calculation of permeability was performed with a spreadsheet by performing a mean between the 4 acquired values.

7 – Results

7.1 – Matrimid

As explained in 5.1.1, Matrimid acquisition were performed in order to validate the experimental bench. The referred Matrimid values were the following [84]:

- $P_{CO_2} = 8.4$ Barrer
- $P_{CH_4} = 0.16$ Barrer
- $t = 25 \mu\text{m}$
- $T = 25^\circ\text{C}$

Permeability results obtained at 20°C with the test bench are shown in *table 7*.

CH4		CO2		SELECTIVITY	
Δp [bar]	P [barrer]	Δp [bar]	P [barrer]	Δp [bar]	α [-]
1	0.089	1	7.98	1	90.0
2	0.179	2	8.41	2	46.9
3	0.133	3	8.09	3	61.0
5	0.156	5	8.06	5	51.7
7	0.157	7	8.36	7	53.2

Table 7: permeability of tested Matrimid membrane to CO2 and CH4 and selectivity.

Obtained results are really similar to the literature ones. Differences between the experiment data and the referred ones could be related to different working temperature and uncertainty of the permeate closed volume in the test rig.

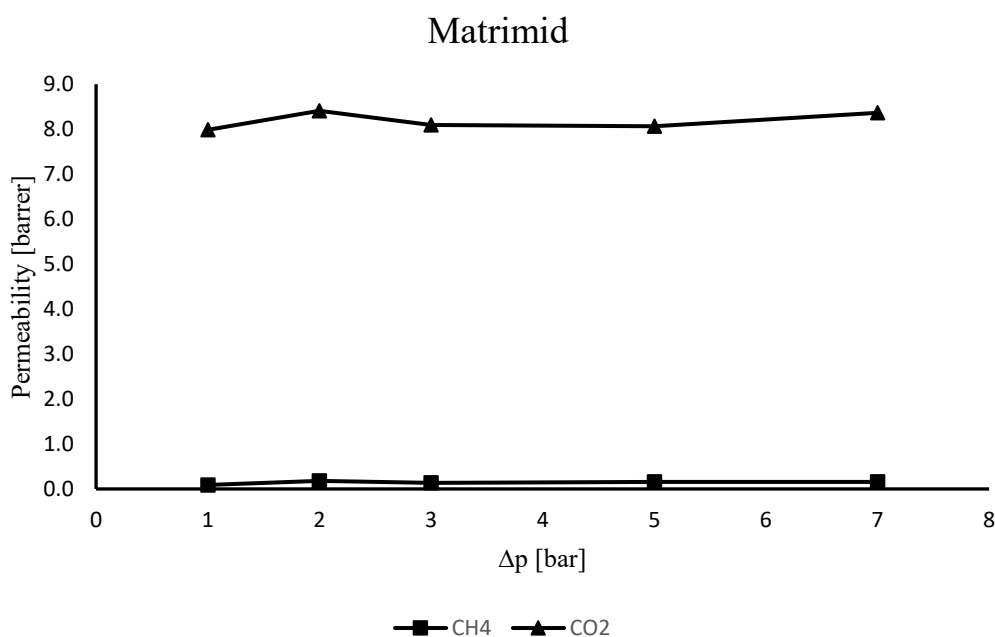


Figure 35: graphical representation of results.

7.2 - PES-WC

As explained in chapter 5, both PES-WC membranes were thermal treated. Main difference is that one of them had a cyclodextrin nanosponge, while the other not. Permeability values are shown in the next sections.

7.2.1 – PES-WC without cyclodextrin nanosponge

Permeability results with PES-WC without nanosponge were many order of magnitude higher than other tested membranes. It follows that membrane tests were performed in open volume setup, in which a volumetric flowmeter was employed.

CH4		CO2		SELECTIVITY	
Δp [bar]	P [barrer]	Δp [bar]	P [barrer]	Δp [bar]	α [-]
1	7.61E+04	1	1.23E+05	1	1.6
2	6.36E+04	2	1.02E+05	2	1.6
3	5.92E+04	3	9.48E+04	3	1.6
4	5.65E+04	4	-	4	-
5	5.51E+04	5	-	5	-
6	5.47E+04	6	-	6	-

Table 8: permeability values of PES-WC without cyclodextrin nanosponge and relative selectivity at different pressure difference.

As it can be seen, maximum tested pressure differences were 6 bar and 3 bar for CH₄ and CO₂ respectively. Volumetric flow reached similar values to instrument FSO at those pressure

differences, hence no more acquisition were performed. Selectivity were evaluated as the ratio between permeability of CO₂ over CH₄.

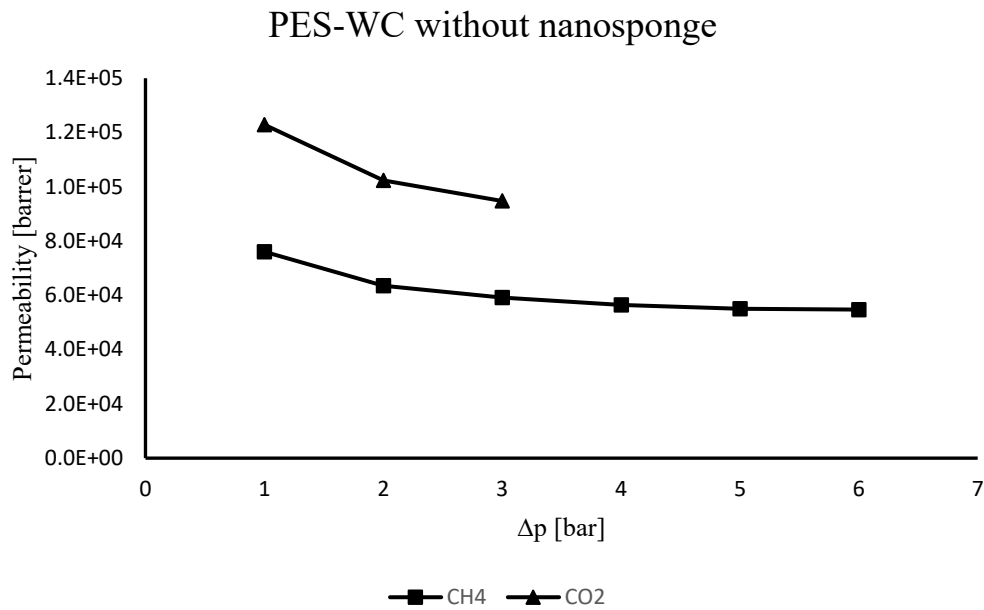


Figure 36: graphical representation of results.

CH₄ line shows a decrease in permeability with the increase of pressure difference, reaching a constant value in the range of pressure difference between 5 bar and 6 bar. In first points CO₂ line has shown similar trend with respect to CH₄ values, which is in accordance with the quite-constant selectivity ratio of 1.6. In both cases, maximum permeability is recorded at the lowest pressure difference measure.

7.2.1 – PES-WC with cyclodextrin nanosponge

PES-WC membrane with cyclodextrin nanosponge results were acquired with the closed volume procedure.

CH4		CO2		SELECTIVITY	
Δp [bar]	P [barrer]	Δp [bar]	P [barrer]	Δp [bar]	α [-]
1	6.76	1	20.38	1	3.02
2	6.07	2	18.74	2	3.09
3	1.53	3	15.30	3	10.01
4	0.92	4	11.02	4	11.92
5	4.36	5	9.87	5	2.26
6	9.43	6	9.01	6	0.96
7	10.78	7	8.27	7	0.77
8	12.33	8	7.78	8	0.63
9	13.14	9	7.61	9	0.58

Table 9: permeabilities and selectivity of PES-WC membrane with cyclodextrin nanosponge.

Acquisition covered pressure difference from 1 bar to 9 bar with 1 bar step each. Main difference with PES-WC without cyclodextrin nanosponge is the order of magnitude of results, which decreased from $10^4 \pm 10^5$ to $10^0 \pm 10^1$.

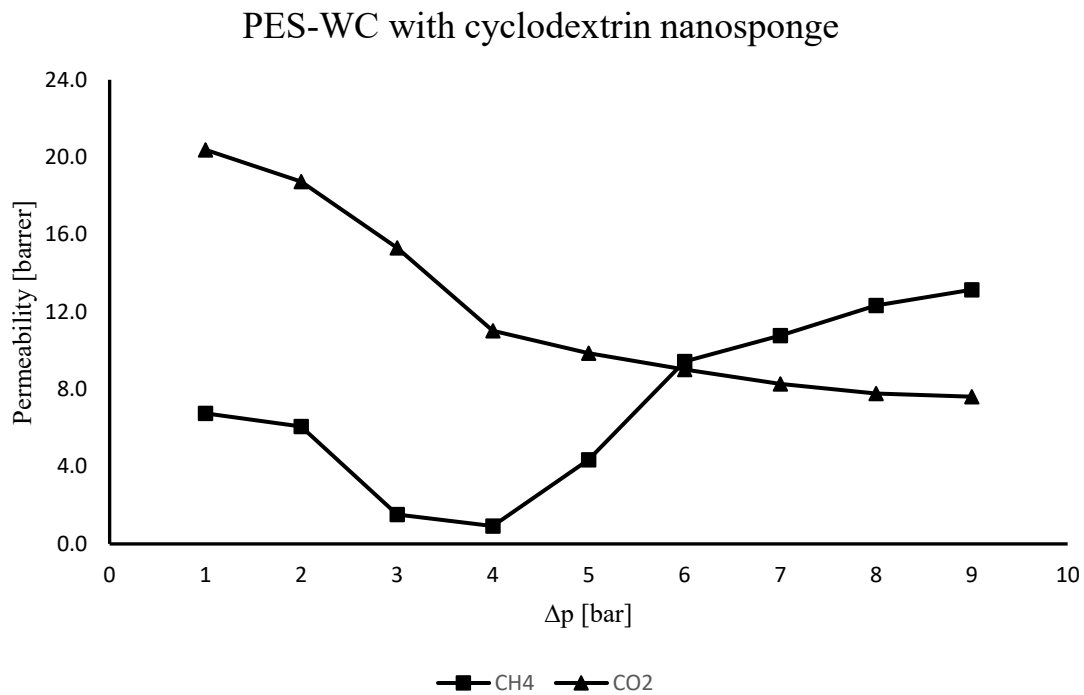


Figure 37: permeability results of CO2 and CH4 for PES-WC with cyclodextrin nanosponge.

For CH₄ permeability line a decrease can be observed from 1 bar to 4 bar, in which it reaches the minimum value; then a sharp increment between 4 bar and 6 bar followed by a light increase in the rest of the range is noted. For CO₂ there is a continuous decrease in permeability with respect to pressure difference, with marked rate between 1 bar and 4 bar.

Selectivity of PES-WC with cyclodextrine nanosponge

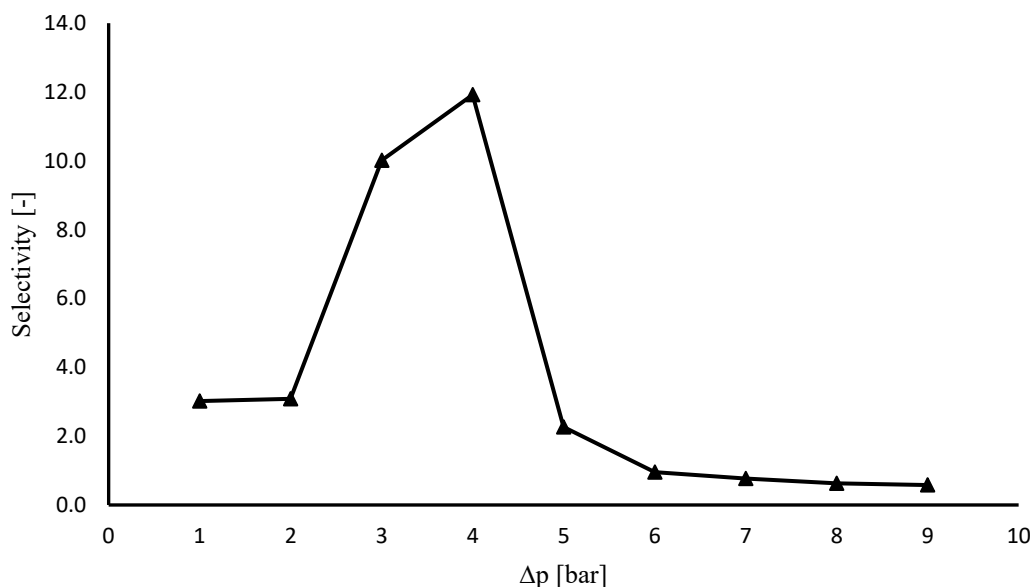


Figure 38: selectivity values for PES-WC membrane with cyclodextrin nanosponge.

From the selectivity point of view, there is a peak at 4 bar due to really low CH_4 permeability value. From 6 bar onwards membrane permeability to CH_4 is higher than the one to CO_2 , which results in selectivity lower than 1.

7.3 - PEEK-WC

PEEK-WC membrane results were acquired with the closed volume procedure.

CH ₄		CO ₂		SELECTIVITY	
Δp [bar]	P [barrer]	Δp [bar]	P [barrer]	Δp [bar]	α [-]
1	0.340	1	1.97	1	5.8
3	0.578	3	1.92	3	3.3
5	0.369	5	1.88	5	5.1
7	0.189	7	2.24	7	11.8

Table 10: permeabilities and selectivities of PEEK-WC to CH_4 and CO_2 .

In tested pressure difference permeability values were an order of magnitude lower than the ones of PES-WC membrane with nanosponge.

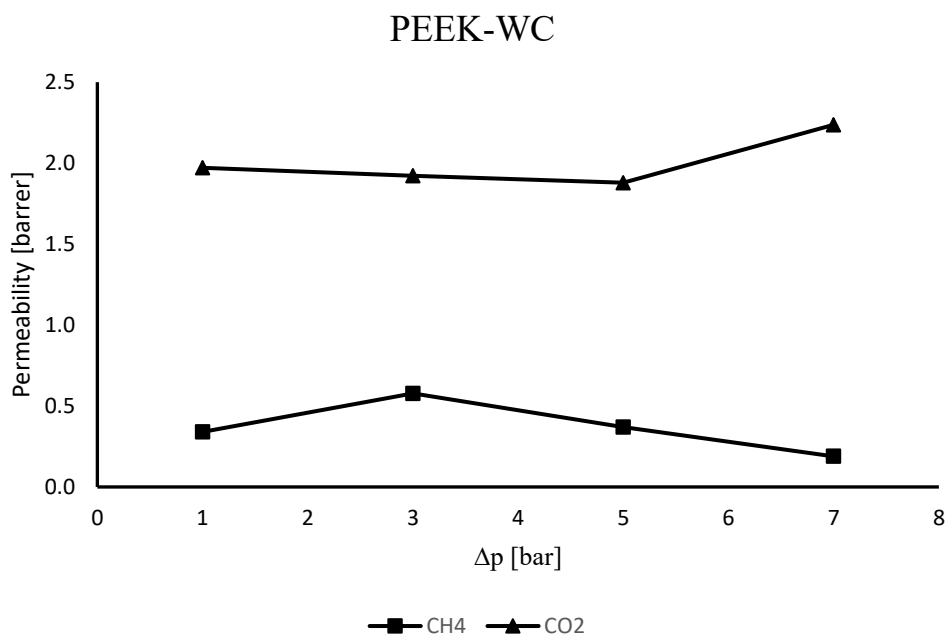


Figure 39: PEEK-WC permeabilities to CH₄ and CO₂

For CH₄ permeability doubled between 1 and 3 bar, in which it reaches the maximum value; then a constant decrease between 3 bar and 7 bar can be observed. With carbon dioxide there is a relatively little change in permeability between 1 bar and 5 bar, while an increase can be seen with a pressure difference of 7 bar.

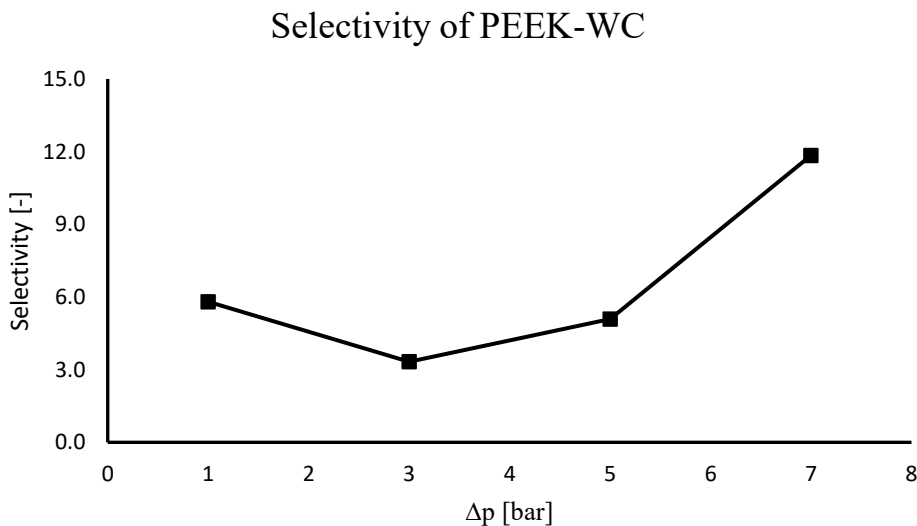


Figure 40: selectivity of PEEK-WC membrane.

Selectivity plot shows a minimum at 3 bar, while gets higher results with the increase of pressure difference across the membrane, reaching a value of 12 at 7 bar.

7.4 – Comparison between tested membranes

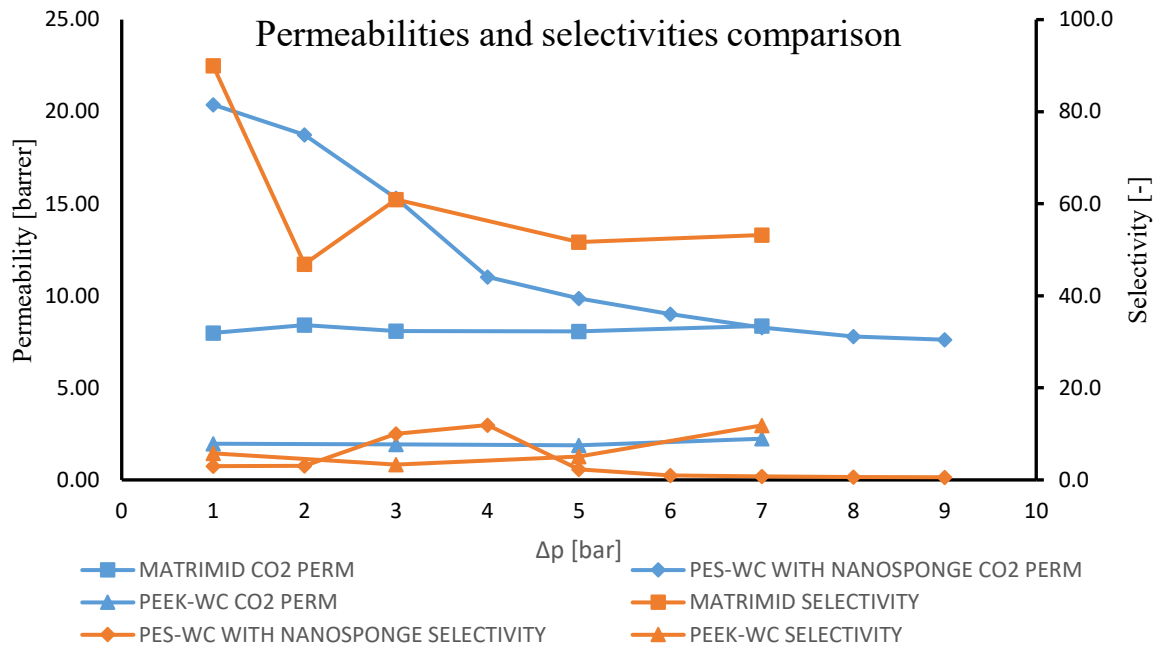


Figure 41: permeabilities (blue lines) and selectivities (orange lines) of tested membranes.

In this comparison it was excluded PES-WC without cyclodextrin nanosponge values due to their different order of magnitude results. With respect to Matrimid membrane, permeability to CO₂ of the other membranes are quite similar and differs less than an order of magnitude. On the other side, looking at selectivities, clearly Matrimid has better performances. While its selectivity in the tested pressure differences is never lower than 40, PES-WC with cyclodextrin nanosponge and PEEK-WC selectivities never reach higher values than 12.

8 – Conclusions

Natural gas has the lowest carbon emission/energy ratio between fossil fuels, a property that led EU to choose it as the energy transition source. Among all the imported gas, Russian NG accounted for 40% share. After the actions against Ukraine in the beginning of 2021, EU dealt with a sharp decrease of NG imports from Russia. Main actions to overcome the lack of NG demand were stipulating new contracts with other suppliers, increase green hydrogen for direct or indirect use (methanation process with carbon dioxide) and enhance biomethane production.

Biomethane is the cleaned and upgraded stream from biogas. Biogas is the product of anaerobic digestion of biological sources, such as organic municipal solid waste and sewage sludge. While cleaning process technologies are engaged in separation of sulphur composites and water from biogas stream, upgrading systems into biomethane are mainly focused on separation of carbon dioxide from CO₂/CH₄ gas mixture.

After an overview of most important gas separation technologies, a study in membrane separation systems was carried out. Solution-diffusion mechanisms, involved materials, Robeson permeability/selectivity curve and main membranes limits were discussed, giving particular attention to polymeric ones. Then a description of four different glassy polymeric dense membrane has been done, i.e. Matrimid, PES-WC, PES-WC with cyclodextrin nanosponge and PEEK-WC. Permeability evaluation of these membranes were performed in CO₂ Circle Lab in Environment Park, Turin.

Matrimid has been used as reference value in order to validate the experimental test bench. Results are in accordance to values found in literature.

PES-WC membrane showed high permeability value in the order of magnitude of $10^4 \pm 10^5$ Barrer and low selectivity between CO₂ and CH₄ (for the tested pressure difference range equal to 1.6). Although PES-WC is a glassy polymer, obtained results show a similar behaviour to a rubbery one.

In the case of PES-WC membrane with cyclodextrin nanosponge, permeability results were between $10^0 \pm 10^1$ Barrer for CO₂ and $10^{-1} \pm 10^0$ Barrer for CH₄, with a value of selectivity equal to 12 when pressure difference between feed and permeate side is equal to 4 bar. On the other side, with higher pressure difference across the membrane, selectivity is drastically reduced. By looking at results, this change mostly depends on the increase in permeability to CH₄ (from 0.92 Barrer to 13.14 Barrer) than the decrease in permeability to CO₂ (from 11.02 Barrer to 7.61 Barrer) in the pressure difference range between 4 bar and 9 bar.

PEEK-WC membrane showed a more linear trend compared to PES-WC membrane with cyclodextrin nanosponge. With pressure differences of 1 bar and 7 bar, permeability to CO₂ showed results of 1.97 Barrer and 2.24 Barrer respectively, with a minimum at 5 bar equal to

1.88 Barrer. This increase in permeability with an increase from 5 bar to 7 bar of pressure difference can be related to plasticization phenomena, an alteration of polymeric structure due to the swelling caused by dissolved CO₂.

In this work, all results obtained with PES-WC, PES-WC with cyclodextrin nanosponge and PEEK-WC membranes could not be directly compared with similar performance values in literature. Performances are highly dependent on composition, physical structure, thermal treatment procedure, working pressure and operative temperature, hence, for example, chemical structure is a necessary condition, but it is not sufficient. In the case of the Matrimid membrane, most of variables matched with literature reference, thus a direct comparison has been done.

Finally, further experiments could be conducted with the same membranes. The aim in this work was to evaluate performances of idle samples with different working pressure at constant temperature. A different experiment could be performed at higher temperature, by setting working condition similar to a real case scenario. Another one could be the test of aging at different pressures: this kind of experiment would evaluate one of the most relevant issue related to polymeric membranes, which is the decrease in performance in a short time relatively to affirmed technologies in carbon capture field.

9 – Bibliography

- [1] IPCC, *Global Warming of 1.5°C*. Cambridge University Press, 2022. doi: 10.1017/9781009157940.
- [2] “Hannah Ritchie, Max Roser and Pablo Rosado (2020) - ‘CO₂ and Greenhouse Gas Emissions’”. Published online at OurWorldInData.org. Retrieved from: ‘<https://ourworldindata.org/co2-and-other-greenhouse-gas-emissions>’ [Online Resource].”
- [3] Unfccc, “ADOPTION OF THE PARIS AGREEMENT - Paris Agreement text English.”
- [4] J. A. Leggett and R. K. Lattanzio, “CRS Report for Congress An Overview of Greenhouse Gas (GHG) Control Policies in Various Countries Specialist in Energy and Environmental Policy,” 2009. [Online]. Available: www.crs.gov
- [5] *Energy Terminology*. Elsevier, 1986. doi: 10.1016/C2009-0-14703-7.
- [6] “World Energy Outlook 2022.” [Online]. Available: www.iea.org/t&c/
- [7] “REPowerEU Plan,” Brussels, May 2022.
- [8] “REPowerEU Plan - Annexes,” Brussels, May 2022.
- [9] A. Tripodi, F. Conte, and I. Rossetti, “Carbon Dioxide Methanation: Design of a Fully Integrated Plant,” *Energy & Fuels*, vol. 34, no. 6, pp. 7242–7256, Jun. 2020, doi: 10.1021/acs.energyfuels.0c00580.
- [10] G. Bahgat, *Energy Security: An Interdisciplinary Approach*. New York, UNITED KINGDOM: John Wiley & Sons, Incorporated, 2011. [Online]. Available: <http://ebookcentral.proquest.com/lib/polito-ebooks/detail.action?docID=792452>
- [11] R. Uddin, H. Raza Khan, A. Arfeen, M. A. Shirazi, A. Rashid, and U. Shahbaz Khan, “Energy Storage for Energy Security and Reliability through Renewable Energy Technologies: A New Paradigm for Energy Policies in Turkey and Pakistan,” *Sustainability*, vol. 13, no. 5, p. 2823, Mar. 2021, doi: 10.3390/su13052823.
- [12] P. Tsvetkov, A. Cherepovitsyn, and S. Fedoseev, “The Changing Role of CO₂ in the Transition to a Circular Economy: Review of Carbon Sequestration Projects,” *Sustainability*, vol. 11, no. 20, 2019, doi: 10.3390/su11205834.

- [13] Ellen MacArthur Foundation, “TOWARDS THE CIRCULAR ECONOMY,” 2013.
- [14] L. M. Alsarhan, A. S. Alayyar, N. B. Alqahtani, and N. H. Khdayr, “Circular Carbon Economy (CCE): A Way to Invest CO₂ and Protect the Environment, a Review,” *Sustainability*, vol. 13, no. 21, p. 11625, Oct. 2021, doi: 10.3390/su132111625.
- [15] R. Chauvy and G. de Weireld, “CO₂ Utilization Technologies in Europe: A Short Review,” *Energy Technology*, vol. 8, no. 12, p. 2000627, Dec. 2020, doi: 10.1002/ente.202000627.
- [16] C. Zhang *et al.*, “Direct conversion of carbon dioxide to liquid fuels and synthetic natural gas using renewable power: Techno-economic analysis,” *Journal of CO₂ Utilization*, vol. 34, pp. 293–302, Dec. 2019, doi: 10.1016/j.jcou.2019.07.005.
- [17] J. R. Centre, I. for E. and Transport, E. Tzimas, T. Sveen, M. Perez Fortes, and A. Bocin-Dumitriu, *Carbon capture and utilisation workshop: background and proceedings*. Publications Office, 2014. doi: doi/10.2790/11560.
- [18] D. Zhang, Z. Ghoulah, and Y. Shao, “Review on carbonation curing of cement-based materials,” *Journal of CO₂ Utilization*, vol. 21, pp. 119–131, Oct. 2017, doi: 10.1016/j.jcou.2017.07.003.
- [19] M. A. Kassim and T. K. Meng, “Carbon dioxide (CO₂) biofixation by microalgae and its potential for biorefinery and biofuel production,” *Science of The Total Environment*, vol. 584–585, pp. 1121–1129, Apr. 2017, doi: 10.1016/j.scitotenv.2017.01.172.
- [20] K. Parthasarathi and L. S. Ranganathan, “Longevity of microbial and enzyme activity and their influence on NPK content in pressmud vermicasts,” *Eur J Soil Biol*, vol. 35, no. 3, pp. 107–113, Jul. 1999, doi: 10.1016/S1164-5563(00)00114-X.
- [21] M. Mahdaviara *et al.*, “Toward smart schemes for modeling CO₂ solubility in crude oil: Application to carbon dioxide enhanced oil recovery,” *Fuel*, vol. 285, p. 119147, Feb. 2021, doi: 10.1016/j.fuel.2020.119147.
- [22] European Commission, “IMPLEMENTING THE REPOWER EU ACTION PLAN: INVESTMENT NEEDS, HYDROGEN ACCELERATOR AND ACHIEVING THE BIO-METHANE TARGETS,” Brussels, May 2022.
- [23] European Commission, “DIRECTIVE OF THE EUROPEAN PARLIAMENT AND OF THE COUNCIL amending Directive (EU) 2018/2001 of the European Parliament and of the Council, Regulation (EU) 2018/1999 of the European Parliament and of the Council and Directive 98/70/EC of the European Parliament and of the Council as

regards the promotion of energy from renewable sources, and repealing Council Directive (EU) 2015/652,” 2021.

- [24] G. Noble Denton *et al.*, “GAS QUALITY HARMONISATION COST BENEFIT ANALYSIS Gas Quality Harmonisation_ Cost Benefit Analysis Report Approved Contact details Name Email Telephone,” 2012.
- [25] IEA, “Outlook for biogas and Prospects for organic growth World Energy Outlook Special Report biomethane,” 2020.
- [26] EBA, “Statistical Report 2022. Tracking biogas and biomethane deployment across Europe,” 2022.
- [27] G. Collins, E. D. van Hullebusch, G. Esposito, C. Carliell-Marquet, and F. G. Feroso, Eds., *Anaerobic Digestion*. Frontiers Media SA, 2018. doi: 10.3389/978-2-88945-679-6.
- [28] D. Andriani, A. Wresta, T. D. Atmaja, and A. Saepudin, “A Review on Optimization Production and Upgrading Biogas Through CO₂ Removal Using Various Techniques,” *Appl Biochem Biotechnol*, vol. 172, no. 4, pp. 1909–1928, Feb. 2014, doi: 10.1007/s12010-013-0652-x.
- [29] I. Angelidaki *et al.*, “Biogas Upgrading: Current and Emerging Technologies,” in *Biofuels: Alternative Feedstocks and Conversion Processes for the Production of Liquid and Gaseous Biofuels*, Elsevier, 2019, pp. 817–843. doi: 10.1016/B978-0-12-816856-1.00033-6.
- [30] R. Kapoor *et al.*, “Advances in biogas valorization and utilization systems: A comprehensive review,” *J Clean Prod*, vol. 273, p. 123052, Nov. 2020, doi: 10.1016/j.jclepro.2020.123052.
- [31] R. Salamat, H. Scaar, F. Weigler, W. Berg, and J. Mellmann, “Drying of biogas digestate: A review with a focus on available drying techniques, drying kinetics, and gaseous emission behavior,” *Drying Technology*, vol. 40, no. 1, pp. 5–29, Jan. 2022, doi: 10.1080/07373937.2020.1781879.
- [32] I. Ullah Khan *et al.*, “Biogas as a renewable energy fuel – A review of biogas upgrading, utilisation and storage,” *Energy Convers Manag*, vol. 150, pp. 277–294, Oct. 2017, doi: 10.1016/j.enconman.2017.08.035.
- [33] P. Cozma, W. Wukovits, I. Mamaliga, A. Friedl, and M. Gavrilesco, “Modeling and simulation of high pressure water scrubbing technology applied for biogas upgrading,”

- Clean Technol Environ Policy*, vol. 17, no. 2, pp. 373–391, Feb. 2015, doi: <https://doi.org/10.1007/s10098-014-0787-7>.
- [34] P. Rotunno, A. Lanzini, and P. Leone, “Energy and economic analysis of a water scrubbing based biogas upgrading process for biomethane injection into the gas grid or use as transportation fuel,” *Renew Energy*, vol. 102, pp. 417–432, Mar. 2017, doi: 10.1016/j.renene.2016.10.062.
- [35] L. Tock, M. Gassner, and F. Maréchal, “Thermochemical production of liquid fuels from biomass: Thermo-economic modeling, process design and process integration analysis,” *Biomass Bioenergy*, vol. 34, no. 12, pp. 1838–1854, Dec. 2010, doi: 10.1016/j.biombioe.2010.07.018.
- [36] F. Meng, Y. Meng, T. Ju, S. Han, L. Lin, and J. Jiang, “Research progress of aqueous amine solution for CO₂ capture: A review,” *Renewable and Sustainable Energy Reviews*, vol. 168, p. 112902, Oct. 2022, doi: 10.1016/j.rser.2022.112902.
- [37] S. Vaz, A. P. Rodrigues de Souza, and B. E. Lobo Baeta, “Technologies for carbon dioxide capture: A review applied to energy sectors,” *Clean Eng Technol*, vol. 8, p. 100456, Jun. 2022, doi: 10.1016/j.clet.2022.100456.
- [38] M. H. V. Bahrún, A. Bono, N. Othman, and M. A. A. Zaini, “Carbon dioxide removal from biogas through pressure swing adsorption – A review,” *Chemical Engineering Research and Design*, vol. 183, pp. 285–306, Jul. 2022, doi: 10.1016/j.cherd.2022.05.012.
- [39] “<https://www.biocycle.net/basics-biogas-upgrading/>.”
- [40] H. Vogtenhuber, R. Hofmann, F. Helminger, and G. Schöny, “Process simulation of an efficient temperature swing adsorption concept for biogas upgrading,” *Energy*, vol. 162, pp. 200–209, Nov. 2018, doi: 10.1016/j.energy.2018.07.193.
- [41] B. Verougstraete *et al.*, “Electrical swing adsorption on 3D-printed activated carbon monoliths for CO₂ capture from biogas,” *Sep Purif Technol*, vol. 299, p. 121660, Oct. 2022, doi: 10.1016/j.seppur.2022.121660.
- [42] B. Aghel, S. Behaein, S. Wongwises, and M. S. Shadloo, “A review of recent progress in biogas upgrading: With emphasis on carbon capture,” *Biomass Bioenergy*, vol. 160, p. 106422, May 2022, doi: 10.1016/j.biombioe.2022.106422.
- [43] J.-L. Li and B.-H. Chen, “Review of CO₂ absorption using chemical solvents in hollow fiber membrane contactors,” *Sep Purif Technol*, vol. 41, no. 2, pp. 109–122, Feb. 2005, doi: 10.1016/j.seppur.2004.09.008.

- [44] R. Wang, D. F. Li, C. Zhou, M. Liu, and D. T. Liang, "Impact of DEA solutions with and without CO₂ loading on porous polypropylene membranes intended for use as contactors," *J Memb Sci*, vol. 229, no. 1–2, pp. 147–157, Feb. 2004, doi: 10.1016/j.memsci.2003.10.022.
- [45] Y. Zhang, J. Sunarso, S. Liu, and R. Wang, "Current status and development of membranes for CO₂/CH₄ separation: A review," *International Journal of Greenhouse Gas Control*, vol. 12, pp. 84–107, Jan. 2013, doi: 10.1016/j.ijggc.2012.10.009.
- [46] M. Mulder, *Basic Principles of Membrane Technology*. Dordrecht: Springer Netherlands, 1996. doi: 10.1007/978-94-009-1766-8.
- [47] J. K. Adewole, A. L. Ahmad, S. Ismail, and C. P. Leo, "Current challenges in membrane separation of CO₂ from natural gas: A review," *International Journal of Greenhouse Gas Control*, vol. 17, pp. 46–65, Sep. 2013, doi: 10.1016/j.ijggc.2013.04.012.
- [48] S. Kanehashi and K. Nagai, "Analysis of dual-mode model parameters for gas sorption in glassy polymers," *J Memb Sci*, vol. 253, no. 1–2, pp. 117–138, May 2005, doi: 10.1016/j.memsci.2005.01.003.
- [49] H. A. Mannan, H. Mukhtar, T. Murugesan, R. Nasir, D. F. Mohshim, and A. Mushtaq, "Recent Applications of Polymer Blends in Gas Separation Membranes," *Chem Eng Technol*, vol. 36, no. 11, pp. 1838–1846, Nov. 2013, doi: 10.1002/ceat.201300342.
- [50] L. S. Lai, Y. F. Yeong, K. Keong Lau, and M. S. Azmi, "Zeolitic Imidazolate Frameworks (ZIF): A Potential Membrane for CO₂/CH₄ Separation," *Sep Sci Technol*, vol. 49, no. 10, pp. 1490–1508, Jul. 2014, doi: 10.1080/01496395.2014.903281.
- [51] E. J. Granite and T. O'Brien, "Review of novel methods for carbon dioxide separation from flue and fuel gases," *Fuel Processing Technology*, vol. 86, no. 14–15, pp. 1423–1434, Oct. 2005, doi: 10.1016/j.fuproc.2005.01.001.
- [52] J. Zhu *et al.*, "Facile hydrogen/nitrogen separation through graphene oxide membranes supported on YSZ ceramic hollow fibers," *J Memb Sci*, vol. 535, pp. 143–150, Aug. 2017, doi: 10.1016/j.memsci.2017.04.032.
- [53] X. Yin, N. Chu, J. Yang, J. Wang, and Z. Li, "Thin zeolite T/carbon composite membranes supported on the porous alumina tubes for CO₂ separation," *International Journal of Greenhouse Gas Control*, vol. 15, pp. 55–64, Jul. 2013, doi: 10.1016/j.ijggc.2013.01.032.

- [54] S. B. Messaoud, A. Takagaki, T. Sugawara, R. Kikuchi, and S. T. Oyama, “Alkylamine–silica hybrid membranes for carbon dioxide/methane separation,” *J Memb Sci*, vol. 477, pp. 161–171, Mar. 2015, doi: 10.1016/j.memsci.2014.12.022.
- [55] T. T. Moore, R. Mahajan, D. Q. Vu, and W. J. Koros, “Hybrid membrane materials comprising organic polymers with rigid dispersed phases,” *AIChE Journal*, vol. 50, no. 2, pp. 311–321, Feb. 2004, doi: 10.1002/aic.10029.
- [56] M. A. Aroon, A. F. Ismail, T. Matsuura, and M. M. Montazer-Rahmati, “Performance studies of mixed matrix membranes for gas separation: A review,” *Sep Purif Technol*, vol. 75, no. 3, pp. 229–242, Nov. 2010, doi: 10.1016/j.seppur.2010.08.023.
- [57] M. Wang, Z. Wang, S. Zhao, J. Wang, and S. Wang, “Recent advances on mixed matrix membranes for CO₂ separation,” *Chin J Chem Eng*, vol. 25, no. 11, pp. 1581–1597, Nov. 2017, doi: 10.1016/j.cjche.2017.07.006.
- [58] Y. Dai *et al.*, “Imidazole functionalized graphene oxide/PEBAX mixed matrix membranes for efficient CO₂ capture,” *Sep Purif Technol*, vol. 166, pp. 171–180, Jun. 2016, doi: 10.1016/j.seppur.2016.04.038.
- [59] N. N. R. Ahmad, C. P. Leo, A. W. Mohammad, N. Shaari, and W. L. Ang, “Recent progress in the development of ionic liquid-based mixed matrix membrane for CO₂ separation: A review,” *Int J Energy Res*, vol. 45, no. 7, pp. 9800–9830, Jun. 2021, doi: 10.1002/er.6518.
- [60] D. Q. Vu, W. J. Koros, and S. J. Miller, “Mixed matrix membranes using carbon molecular sieves,” *J Memb Sci*, vol. 211, no. 2, pp. 311–334, Jan. 2003, doi: 10.1016/S0376-7388(02)00429-5.
- [61] F. A. H. Juber, Z. A. Jawad, B. L. F. Chin, S. P. Yeap, and T. L. Chew, “The prospect of synthesis of PES/PEG blend membranes using blend NMP/DMF for CO₂/N₂ separation,” *Journal of Polymer Research*, vol. 28, no. 5, p. 177, May 2021, doi: 10.1007/s10965-021-02500-6.
- [62] M. Sarfraz, “Carbon Capture via Mixed-Matrix Membranes Containing Nanomaterials and Metal–Organic Frameworks,” 2020, pp. 45–94. doi: 10.1007/978-3-030-33978-4_2.
- [63] T. Masuda, E. Isobe, T. Higashimura, and K. Takada, “Poly[1-(trimethylsilyl)-1-propyne]: a new high polymer synthesized with transition-metal catalysts and characterized by extremely high gas permeability,” *J Am Chem Soc*, vol. 105, no. 25, pp. 7473–7474, Nov. 1983, doi: 10.1021/ja00363a061.

- [64] H. B. Park, J. Kamcev, L. M. Robeson, M. Elimelech, and B. D. Freeman, “Maximizing the right stuff: The trade-off between membrane permeability and selectivity,” *Science (1979)*, vol. 356, no. 6343, Jun. 2017, doi: 10.1126/science.aab0530.
- [65] B. Comesaña-Gándara *et al.*, “Redefining the Robeson upper bounds for CO₂/CH₄ and CO₂/N₂ separations using a series of ultrapermeable benzotriptycene-based polymers of intrinsic microporosity,” *Energy Environ Sci*, vol. 12, no. 9, pp. 2733–2740, 2019, doi: 10.1039/C9EE01384A.
- [66] L. M. Robeson, “The upper bound revisited,” *J Memb Sci*, vol. 320, no. 1–2, pp. 390–400, Jul. 2008, doi: 10.1016/j.memsci.2008.04.030.
- [67] P. J. Flory and H. Shih, “Thermodynamics of Solutions of Poly(dimethylsiloxane) in Benzene, Cyclohexane, and Chlorobenzene,” *Macromolecules*, vol. 5, no. 6, pp. 761–766, Nov. 1972, doi: 10.1021/ma60030a019.
- [68] K. Ebert, J. Koll, M. F. J. Dijkstra, and M. Eggers, “Fundamental studies on the performance of a hydrophobic solvent stable membrane in non-aqueous solutions,” *J Memb Sci*, vol. 285, no. 1–2, pp. 75–80, Nov. 2006, doi: 10.1016/j.memsci.2006.07.037.
- [69] M. S. Suleman, K. K. Lau, and Y. F. Yeong, “Plasticization and Swelling in Polymeric Membranes in CO₂ Removal from Natural Gas,” *Chem Eng Technol*, vol. 39, no. 9, pp. 1604–1616, Sep. 2016, doi: 10.1002/ceat.201500495.
- [70] N. Du, M. M. Dal-Cin, G. P. Robertson, and M. D. Guiver, “Decarboxylation-Induced Cross-Linking of Polymers of Intrinsic Microporosity (PIMs) for Membrane Gas Separation,” *Macromolecules*, vol. 45, no. 12, pp. 5134–5139, Jun. 2012, doi: 10.1021/ma300751s.
- [71] Z.-A. Qiao *et al.*, “Polymeric molecular sieve membranes via in situ cross-linking of non-porous polymer membrane templates,” *Nat Commun*, vol. 5, no. 1, p. 3705, Apr. 2014, doi: 10.1038/ncomms4705.
- [72] P. Pandey, R. S. Chauhan, and A. K. Shrivastava, “Carbon-dioxide-induced plasticization effects in solvent-cast polyethylene membranes,” *J Appl Polym Sci*, vol. 83, no. 12, pp. 2727–2731, Mar. 2002, doi: 10.1002/app.10228.
- [73] D. F. Sanders *et al.*, “Energy-efficient polymeric gas separation membranes for a sustainable future: A review,” *Polymer (Guildf)*, vol. 54, no. 18, pp. 4729–4761, Aug. 2013, doi: 10.1016/j.polymer.2013.05.075.

- [74] D. W. Wallace, J. Williams, C. Staudt-Bickel, and W. J. Koros, "Characterization of crosslinked hollow fiber membranes," *Polymer (Guildf)*, vol. 47, no. 4, pp. 1207–1216, Feb. 2006, doi: 10.1016/j.polymer.2005.12.079.
- [75] K. Vanherck, G. Koeckelberghs, and I. F. J. Vankelecom, "Crosslinking polyimides for membrane applications: A review," *Prog Polym Sci*, vol. 38, no. 6, pp. 874–896, Jun. 2013, doi: 10.1016/j.progpolymsci.2012.11.001.
- [76] J. K. Adewole, A. L. Ahmad, S. Ismail, and C. P. Leo, "Current challenges in membrane separation of CO₂ from natural gas: A review," *International Journal of Greenhouse Gas Control*, vol. 17, pp. 46–65, Sep. 2013, doi: 10.1016/j.ijggc.2013.04.012.
- [77] H. A. Mannan, H. Mukhtar, T. Murugesan, R. Nasir, D. F. Mohshim, and A. Mushtaq, "Recent Applications of Polymer Blends in Gas Separation Membranes," *Chem Eng Technol*, vol. 36, no. 11, pp. 1838–1846, Nov. 2013, doi: 10.1002/ceat.201300342.
- [78] H. A. Mannan, H. Mukhtar, and T. Murugesan, "Preparation and Characterization of Newly Developed Polysulfone/Polyethersulfone Blend Membrane for CO₂ Separation," *Applied Mechanics and Materials*, vol. 699, pp. 325–330, Nov. 2014, doi: 10.4028/www.scientific.net/AMM.699.325.
- [79] A. BHATTACHARYA, "Grafting: a versatile means to modify polymers Techniques, factors and applications," *Prog Polym Sci*, vol. 29, no. 8, pp. 767–814, Aug. 2004, doi: 10.1016/j.progpolymsci.2004.05.002.
- [80] R. Checchetto, M. Scarpa, M. G. de Angelis, and M. Minelli, "Mixed gas diffusion and permeation of ternary and quaternary gas mixtures in Matrimid®, polyetherimide and poly(lactic acid) membranes for separation," *J Memb Sci*, vol. 659, p. 120768, Oct. 2022, doi: 10.1016/j.memsci.2022.120768.
- [81] G. C. Kapantaidakis and G. H. Koops, "High flux polyethersulfone–polyimide blend hollow fiber membranes for gas separation," *J Memb Sci*, vol. 204, no. 1–2, pp. 153–171, Jul. 2002, doi: 10.1016/S0376-7388(02)00030-3.
- [82] M. Loloie, M. Omidkhah, A. Moghadassi, and A. E. Amooghin, "Preparation and characterization of Matrimid® 5218 based binary and ternary mixed matrix membranes for CO₂ separation," *International Journal of Greenhouse Gas Control*, vol. 39, pp. 225–235, Aug. 2015, doi: 10.1016/j.ijggc.2015.04.016.
- [83] R. Castro-Muñoz, V. Martín-Gil, M. Z. Ahmad, and V. Fíla, "Matrimid® 5218 in preparation of membranes for gas separation: Current state-of-the-art," *Chem Eng Commun*, vol. 205, no. 2, pp. 161–196, Feb. 2018, doi: 10.1080/00986445.2017.1378647.

- [84] L. Ansaloni, M. Minelli, M. Giacinti Baschetti, and G. C. Sarti, "Effect of relative humidity and temperature on gas transport in Matrimid®: Experimental study and modeling," *J Memb Sci*, vol. 471, pp. 392–401, Dec. 2014, doi: 10.1016/j.memsci.2014.08.019.
- [85] A. P. Sherje, B. R. Dravyakar, D. Kadam, and M. Jadhav, "Cyclodextrin-based nanosponges: A critical review," *Carbohydr Polym*, vol. 173, pp. 37–49, Oct. 2017, doi: 10.1016/j.carbpol.2017.05.086.
- [86] J. C. Jansen and E. Drioli, "Poly(ether ether ketone) derivative membranes—a review of their preparation, properties and potential," *Polymer Science Series A*, vol. 51, no. 11–12, pp. 1355–1366, Dec. 2009, doi: 10.1134/S0965545X09110200.

